Scaling of Structural and Rheological Response of L_3 Sponge Phases in the "Sweetened" Cetylpyridinium/ Hexanol/Dextrose/Brine System

L. Porcar,* W. A. Hamilton, and P. D. Butler

Condensed Matter Sciences Division, Oak Ridge National Laboratory, Oak Ridge, Tennessee 37831

G. G. Warr

University of Sydney, School of Chemistry, Sydney, NSW 2006, Australia

Received April 17, 2003. In Final Form: August 21, 2003

We report a study of the shear response of sponge phases in cetylpyridinium chloride (CPCl)/hexanol/brine/dextrose systems by parallel measurements of rheology and structure by small angle neutron scattering (SANS). Our measurements show that this dextrose added to the extensively studied CPCl/hexanol/brine system is taken up exclusively by the brine solvent, resulting in an equivalent CPCl/hexanol membrane structure and phase behavior for this modified system. Adding dextrose to the brine in these systems to volume fractions up to 0.4 allows us to increase the solvent viscosity by more than an order of magnitude. This lowers the cooperative membrane diffusion coefficient in this system as measured by dynamic light scattering by the same factor, resulting in a corresponding slowing of the Helfrich fluctuation dominated membrane dynamics. Our results show clear and consistent evidence of shear-induced sponge to lamellar phase transformations in these systems. Further, both the rheological and microstructural responses of these systems follow universal master curves when plotted against a rescaled applied shear $\dot{\gamma}\eta_s/\phi^3$, where ϕ is the membrane volume fraction and η_s is the viscosity of the brine/dextrose solvent. This well-defined shear response is characterized by three distinct regimes. At low shear rates the sponge phases exhibit Newtonian flow behavior and no structural change is observed. For intermediate shear rates, the systems shear thin and SANS measurements show that the sponge phases are progressively transformed into lamellar phases with the CPCl/hexanol membrane normals aligned parallel to the velocity gradient. This continuous process and the absence of a stress plateau in the rheological measurements both rule out the existence of a biphasic state in this region and thus of a first-order transition between sponge and lamellar phases as is observed in equilibrium phase diagrams. At higher shear rates, the systems are apparently again Newtonian, but the induced lamellar phase appears to collapse and a new (and as yet unidentified) large-scale structure forms. We have found these systems to be extremely sensitive to evaporation, and reproducibility of the scattering measurements required the use of a Couette shear cell with a specially designed vapor barrier.

Introduction

For many years shear-induced structural transformation and ordering in complex fluids such as polymers, surfactant solutions, and liquid crystals have been extensively studied for both scientific and industrial reasons. As the length scales directly controllable by technological means have grown smaller, there has been a convergence of practical and fundamental interests toward a common aim: the understanding of the microstructural response as correlated with macroscopic rheological behavior.[1]

Depending on characteristic structural relaxation times, shear flow can produce the familiar viscous heating of simple liquids[2] or more dramatic "complex" effects at odds with our usual expectations of fluid behavior: both macroscopically, as in the anisotropic rheological responses of viscoelastic liquids, and microscopically, in phenomena such as shear melting[3] or crystallization.[4−6] To a large extent what makes a fluid complex is an extended structural organization such as that exhibited by long polymer chains or the self-assembled threadlike micelles and membranes in surfactant systems. Processes acting over these longer length scales are slower and more easily disrupted by normally accessible shears. Interactions with the shear flow field can then induce either structural perturbations or full-blown phase changes, which in their turn affect the viscosity and shear response of the fluid.

The rich variety of responses of membrane phases to shear flow has attracted a great deal of attention in the past few years. The most widely processed and studied membrane mesophase is undoubtedly the smectic lamellar L_α phase (Figure 1), which is observed in nonionic, anionic, cationic, and zwitterionic surfactant systems as well as in block copolymers. Under steady shear, L_α phases display three different stationary states.[7,8] The perpendicular "a" orientation corresponds to membranes with their normals aligned parallel to the vorticity direction; the transverse

* Current address: National Institute for Standards and Technology Center for Neutron Research, Gaithersburg, MD 20899.

(1) Butler, P. D. *Curr. Opin. Colloid Interface Sci.* **1999**, *4*, 214 and references therein.
(2) Macosko, C. W. *Rheology: principles, measurements and applications*; Wiley-VCH: New York, 1994.
(3) Ackerson, B. J.; Clark, N. *Phys. Rev. A* **1984**, *30*, 906.
(4) Hamilton, W. A.; Butler, P. D.; Magid, L. J.; Han, Z.; Slawecki, T. M. *Phys. Rev. E* **1999**, *60* (2), R1146.
(5) Panine, P.; Narayanan, T.; Vermant, J.; Mewis, J. *Phys. Rev. E* **2002**, *66* (2), art. no. 022401 Part 1.
(6) Slawecki, T. M.; Glinka, G. J.; Hammouda, B. *Phys. Rev. E* **1998**, *58* (4), R4084.
(7) Miecowicz, M. *Nature* **1946**, *158*, 27.
(8) Safinya, C. R.; Sirota, E. B.; Bruinsma, R. F.; Jeppesen, C.; Plano, R. J.; Wenzel, L. J. *Science* **1993**, *261*, 588.

10.1021/la034661w CCC: $25.00
Published on Web 10/11/2003

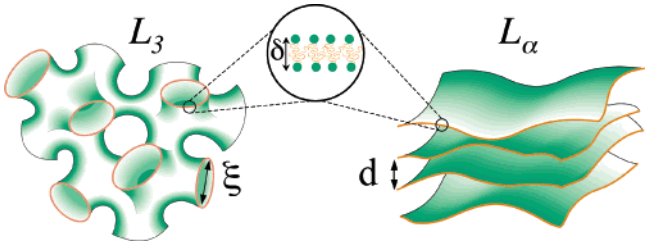

Figure 1. Schematic representation of sponge (L_3) and lamellar (L_α) membrane morphologies and their respective characteristic lengths, the sponge pore size ξ, and lamellar periodicity d. The inset shows an expanded view of a section of the membrane showing the aggregation of surfactant molecules forming the bilayer of thickness δ.

"b" orientation has the normals aligned parallel to the flow; and the parallel "c" orientation has the normals aligned along the velocity gradient direction. In these studies extensive nonequilibrium phase diagrams have been constructed for many systems representing the steady states of the lamellar system under shear.[9,10] In addition to these simply oriented lamellar phases, which have immediate consequences in the processing of polymeric systems, it has also been found that shear flow can induce the formation of more complicated structures. Pioneering studies by Roux and co-workers[9,11,12] showed that prolonged steady shear in a Couette cell may cause a dynamic transition from the L_α smectic phase to multilamellar vesicles, often called "onions" or "spherulites". The possibility of introducing encapsulated particles within or between the layers of the spherulite structure has received considerable attention for delayed release applications in drug delivery, biochemical catalysis, and cosmetic technologies.[13] The size of the vesicles is closely related to the shear rate $\dot{\gamma}$, and under certain conditions of formation, these may be sufficiently monodisperse that they may be ordered in a crystalline phase by further shear.[14−18]

In many systems the isotropic L_3 sponge phase membrane structure is observed in narrow phase regions adjacent to the domain of stability of L_α phases (Figures 1 and 2). These L_3 phases are free flowing, which could make them attractive for mixing or transfer stages in technological processes involving the more viscous neighboring membrane phase. Unlike lamellar and crystalline phases, sponge phases present no long-range order. A number of studies[19] have determined that this phase consists of one infinite membrane bilayer in a convoluted morphology, which is randomly interconnected throughout space and divides the sample volume into two equivalent strongly interwoven subvolumes. The relative stability of the isotropic L_3 and L_α structures depends critically on the membrane curvature and flexibility. In consequence, transitions between these two phases may readily be

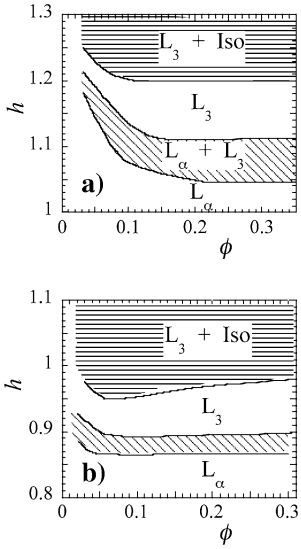

Figure 2. Partial phase diagram at 20 °C of (a) CPCl/hexanol/brine (0.2 M NaCl) and (b) CPCl/hexanol/dextrose/brine (0.2 M NaCl) at a dextrose volume fraction in brine $\psi = 0.4$. ϕ is the membrane volume fraction, and h represents the mass ratio of the hexanol cosurfactant to CPCl. Increasing h corresponds to an increase in the intrinsic curvature of the membrane, which is reflected in the sequence of phases and biphasic regions shown here: stacked lamellar (L_α), sponge (L_3), and isotropic micellar (Iso). This is typical of membrane-forming surfactant phase behavior with respect to a change in such a parameter. Substitution of D_2O for H_2O for contrast in the neutron scattering experiments lowers the values of h at which these phases are observed by about 2% for both these dextrose volume fractions.

induced by altering these membrane properties. Such changes may be achieved by many methods, including varying temperature, electrolyte concentration, and cosurfactant surfactant ratio, all of which have been extensively studied over the past decade.[20−23] More recently it has been shown that structural transformations similar to these bulk isotropic transitions can also be induced by geometrical constraints. The confinement of a sponge phase between two rigid macroscopic walls of a surface forces apparatus can lead to a first-order transition to a lamellar phase,[24,25] which rapidly relaxes when the confinement ceases.

We have recently characterized the ordering of the bulk sponge phase in the proximity of a quartz surface using simultaneous measurement of neutron reflectometry (NR) and near surface small angle neutron scattering (NS-SANS) of a reflection geometry sample cell.[26] The NR results indicate a layered surface ordering correlated with the solid−liquid interface and decaying exponentially with depth over distances corresponding to a few membrane separations. NS-SANS results are consistent with conventional SANS measurements, indicating that the layered ordering established does not constitute a phase of

(9) Diat, O.; Roux, D.; Nallet, F. *J. Phys. II* **1993**, *3*, 1427.
(10) Zipfel, J.; Berghausen, J.; Lindner, P.; Richtering, W. *J. Phys. Chem. B* **1999**, *103*, 2841.
(11) Diat, O.; Roux, D. *J. Phys. II* **1993**, *3*, 9.
(12) Gulik-Krzywicki, T.; Dedieu, J. C.; Roux, D.; Degert, C.; Laversanne, R. *Langmuir* **1996**, *12*, 4668.
(13) Lasic, D. D. *Liposomes*; Elsevier: New York, 1993.
(14) Diat, O.; Roux, D.; Nallet, F. *Phys. Rev. E* **1995**, *51*, N.4, 3296.
(15) Sierro, P.; Roux, D. *Phys. Rev. Lett.* **1997**, *78*, 1496.
(16) Lee, T. D.; Olsson, U.; Mortensen, K. *Phys. Chem. Chem. Phys.* **2001**, *3*, 1310.
(17) Berni, M. G.; Lawrence, C. J.; Machin, D. *Adv. Colloid Interface Sci.* **2002**, *98*, 217.
(18) Courbin, L.; Delville, J. P.; Rouch, J.; Panizza, P. *Phys. Rev. Lett.* **2002**, *89*, 148305.
(19) Porte, G. *J. Phys.: Condens. Matter* **1992**, *4*, 8649 and references therein.
(20) Nastishin, Y.; Lambert, E.; Boltenhagen, P. *C. R. Acad. Sci. Paris* **1995**, *t. 321*, Ser. IIb 205.
(21) Porte, G.; Marignan, J.; Bassereau, P.; May, R. *J. Phys. (Paris)* **1988**, *49*, 511.
(22) Ghosh, O.; Miller, C. A. *J. Phys. Chem.* **1987**, *91*, 4528.
(23) Strey, R.; Jahn, W.; Skouri, M.; Porte, G.; Marignan, J.; Olsson, U. *Structure and Dynamics of strongly Interacting Colloids and Supramolecular Aggregates in Solution*; Chen, S., Huang, J. S., Eds.; Kluwer Academic Publishers: Dordrecht, 1992; p 351.
(24) Antelmi, D. A.; Kekicheff, P.; Richetti, P. *J. Phys. II* **1995**, *5*, 103.
(25) Petrov, P.; Olsson, U.; Christenson, H.; Miklavic, S.; Wennerström, H. *Langmuir* **1994**, *10*, 988.
(26) Hamilton, W. A.; Porcar, L.; Butler, P. D.; Warr, G. G. *J. Chem. Phys.* **2002**, *116*, 8533.

significant volume and is therefore driven by local changes to the free energy at the interface. Similar results were earlier reported by Zhou et al.[27] for bicontinuous $C_{10}E_4$/octane/D_2O microemulsions, a system topologically similar to the sponge phases.

In some sense we expect dynamical responses to shear to be similar to those to the geometric constraint in that they arise from the introduction of anisotropy to a system. The dilute isotropic sponge phases studied here show a striking example of such a dynamical response when, while being gently shaken or stirred, they become birefringent. As is well-known, stacked lamellar phases are strongly birefringent, so this response suggests a shear-induced anisotropic ordering. In their theoretical analysis of the nonequilibrium transitions in complex systems based on the Maxwell effect, Cates and Milner[28] predicted that coupling between the order parameter and the shear flow should shift an observed isotropic to lamellar transition by suppressing fluctuations and thus altering the forces acting to stabilize the isotropic phase. In such an analysis, shear may be viewed as a quasi-thermodynamic variable, since the transformations considered are those between phases that exist in equilibrium. Further, they predicted that the induced phase should occur preferentially in an orientation with the lamellar periodicity normal to both the velocity and the velocity gradient (the a orientation as defined above). These predictions were confirmed experimentally by Koppi et al.,[29] who found a shear-induced shift in the isotropic to lamellar transition temperature in a block copolymer system. Cates and Milner also suggested that shear flow should similarly destabilize the isotropic sponge phase and stabilize the anisotropic lamellar phase, thus neatly explaining the transient birefringent response in these systems.

Such a transition must occur when the time scales for viscous and Brownian motions become comparable, so that the Peclet number[30] is of order unity. The Peclet number is defined here as $Pe = \dot{\gamma}\xi^2/D$, where ξ is the sponge's characteristic length and D is the diffusion coefficient. The diffusion constant for the membrane is given by a Stokes relationship and scales as $D \sim k_B T/\xi\eta_s$, where η_s is the solvent viscosity. Thus, as originally noted by Cates and Milner,[28] the critical shear rate for a transition should scale as $\dot{\gamma}_c \sim k_B T/\xi^3\eta_s$. The correlation length itself scales as $\xi \sim \delta/\phi$, where δ is the membrane thickness—typically ~20 Å—and ϕ is the volume fraction of membrane, so that for a 10% membrane volume fraction sponge phase $\xi \sim$ 200 Å. In a surfactant water system $\eta_s = 1$ cP, and so $\dot{\gamma}_c$ should be about 100 000 s^{-1}. Thus, at moderate concentrations of commonly studied sponge phases, a transition should occur at shear rates nearly an order of magnitude above the highest available experimentally under controlled conditions (~15 000 s^{-1}). However, the strong concentration dependence predicted for $\dot{\gamma}_c$ suggests that experimentally accessible critical shear rates (near or below 10^3 s^{-1}) should occur for very dilute sponge phases (membrane volume fractions < 2%), and indeed transient birefringence under stirring is most easily observed in such low concentration samples.[31]

Taking advantage of this strong concentration dependence by working on a hyperswollen lyotropic $C_{12}E_5$ system, Yamamoto and Tanaka[32] were able to show in light scattering measurements that oscillatory shear flow would suppress the first-order nature of a sponge to lamellar transition, reducing the width of the phase coexistence region. As one would expect from the quasi-thermodynamic characteristics of the predicted transformation, this suppression was fully reversible and disappeared upon cessation of the shearing flow. Total suppression of the transition was observed at an average shear rate $\langle\dot{\gamma}\rangle \sim 300$ s^{-1}, consistent with the expected value of $\dot{\gamma}_c$ calculated for their 1.8% $C_{12}E_5$ in the water sponge phase of 270 s^{-1} (in this case, the membrane thickness $\delta \sim 30$ Å). Also consistent with the scaling prediction were quantitative Couette shear studies of the birefringent response to shear in quaternary sodium dodecyl sulfate (SDS)/pentanol/dodecane/water sponge systems by Diat et al.,[33] which indicated that birefringence occurs above a critical shear rate which increased as the cube of the membrane volume fraction.

However, in a surprising contradiction to this prediction, Majhoub et al.[34] recently reported small-angle X-rays studies apparently indicating that relatively concentrated 10−15% sponge phases in the CPCl/hexanol/brine sponge system could be totally transformed to a lamellar phase under Couette shear at an unexpectedly low critical shear rate of about 50 s^{-1}. This work is obviously at odds with the good agreement found by Yamamoto and Tanaka as well as the failure of other workers to observe such a low shear transition in concentrated sponge phases of this and other systems.[35−37] Even more surprisingly, they claimed that in their case the shear-induced sponge to lamellar transition was apparently not reversible and that the "stabilized" lamellar phase produced in their experiments was never observed to relax to its initial equilibrium sponge phase after shear cessation.

While these reports have reopened the question of shear driven L_3 to L_α transitions of the CPCl/hexanol/brine system in particular and of the dynamics of the transition in general,[38] the conclusions in each case are based on observations of a few specific sponge phase samples. To address the dynamics of these transitions systematically requires a system that may be expected to exhibit this behavior in an experimentally accessible shear regime (if possible well below 10 000 s^{-1}) for the widest possible range of the relevant system parameters. As discussed above, the critical shear rate for a sponge to lamellar transition will be proportional to the cube of the membrane concentration and inversely proportional to the sample viscosity. The strong concentration dependence suggests that a convenient critical shear rate should be achievable by studying dilute samples, as was done by Yamamoto and Tanaka.[32] However, the decreasing width of the sponge phase stability domain with dilution, loss of scattering signal strength of the characteristic sponge cell size

(27) Zhou, X.-L.; Lee, L. T.; Chen, S.-H.; Strey, R. *Phys. Rev. A* **1992**, *46*, 6479.
(28) Cates, M. E.; Milner, S. T. *Phys. Rev. Lett.* **1989**, *62*, 1856.
(29) Koppi, K. A.; Tirrell, M.; Bates, F. S. *Phys. Rev. Lett.* **1993**, *70*, 1449.
(30) Hunter, R. J. *Foundations of Colloid Science Volume I*; Oxford University Press: 1987.
(31) Hoffman, H.; Hofman, S.; Rauscher, A.; Kalus, J. *Prog. Colloid Polym. Sci.* **1991**, *84*, 24.
(32) Yamamoto, J.; Tanaka, H. *Phys. Rev. Lett.* **1996**, *77*, 4390.
(33) Diat, O.; Roux, D. *Langmuir* **1995**, *11*, 1392.
(34) Majhoub, H. F.; Bourgaux, C.; Sergot, P.; Kléman, M. *Phys. Rev. Lett.* **1998**, *81*, 2076.
(35) Porte, G. (private communication).
(36) Butler, P. D.; Porcar, L.; Hamilton, W. A.; Warr, G. G. *Phys. Rev. Lett.* **2002**, *88*, 059601.
(37) Porcar, L.; Hamilton, W. A.; Butler, P. D.; Warr, G. G. *Phys. Rev. Lett.* **2002**, *89*, 168301.
(38) Recently published results (Leon, A.; Bonn, D.; Meunier, J.; Al-Kahwaji, A.; Kellay, H. *Phys. Rev. Lett.* **2001**, *86*, 938) also claim that shear induces a quite extraordinary first-order sponge to lamellar transition for a 7% membrane volume fraction in the AOT/brine system. After a delay time at constant shear rates, random nucleation and growth of a lamellar phase within the sponge phase has been observed. The delay time reported before nucleation was observed decreased as the imposed shear rate increased, but the transition did not depend directly on the shear rate (or the total strain) on the sample.

signature and its movement to lower scattering vector, the difficulty of performing corresponding rheological measurement on these low viscosity solutions, and greatly increased sensitivity to cosurfactant evaporation in the particular case of the CPCl/hexanol/brine system make this option less attractive than it might initially appear.

In the work reported here, to avoid the necessity of measurements on very low membrane volume fraction sponge phases, we have additionally adopted the alternative strategy of increasing the solvent viscosity. We take our lead from work indicating that, in microemulsion systems, adding sugar can achieve this result without altering the form of the phase diagram.[39] Similarly, we find that dissolving dextrose in the brine solvent does not significantly alter the general phase behavior or sponge structure observed for this system. However, it does allow us to increase the solvent viscosity of our sponge phase samples by about an order of magnitude. Simple crossed polarizer observations of these CPCl/hexanol/dextrose/brine sponge solutions at moderate membrane concentrations were extremely promising, showing clear birefringence upon gentle stirring. This was not observed in sugar-free CPCl/hexanol/brine samples at the same membrane volume fractions and indicated a greatly increased shear response and a probable lowering of the critical shear rate for a sponge to lamellar transition for these samples. A further advantage to be expected for these sweetened sponge phases is one of hydrodynamic stability, since the increased viscosity reduces a sample's Reynolds number at a given cell rotation speed, moving the onset of turbulence in the Couette cell to higher shear rates.

Experimental Methods

Materials. Cetylpyridinium chloride (CPCl) was purchased from Sigma and recrystallized twice in acetone. Hexanol (purity > 99.99%), dextrose (purity > 99.9%), and sodium chloride (NaCl purity > 99.99%) were obtained from Sigma-Aldrich and used as received. Water was ultrapure deionized Millipore water. For neutron scattering measurements, water was replaced by heavy water in order to increase the scattering contrast between membrane and solvent. We found that this substitution only slightly changed the phase boundaries reported for light water, with the difference in density apparently acting to compensate for changes in solubility. After weighing and mixing of the surfactant, cosurfactant, water, and dextrose, the sample solutions were stirred and centrifuged several times in order to ensure homogeneity. The samples were then left undisturbed at 20 °C for several days to allow them to reach thermodynamic equilibrium.

We have used the following densities: 0.2 M NaCl in D_2O, 1.107 g/cm^3; 0.2 M NaCl in H_2O, 1.00 g/cm^3; CPCl, 0.98 g/cm^3; hexanol, 0.818 g/cm^3: dextrose, 1.562 g/cm^3. In this work the sample composition is fully described by the following parameters: the membrane volume fraction, $\phi = (V_{CPCl} + V_{hex})/V_{total}$ (the very low solubilities of CPCl and hexanol in water have been neglected); the mass mixing ratio of the membrane, $h = m_{hex}/m_{CPCl}$; and the volume fraction of dextrose in the solvent, $\psi = V_{dextrose}/(V_{dextrose} + V_{brine})$. To minimize spurious evaporation effects, all samples were in the hexanol-rich part of the sponge phase stability domain close to the L_3/Iso (isotropic) boundary. Using samples far away from the L_3/L_α coexistence region reduces their sensitivity to small losses of the hexanol cosurfactant, which might otherwise drive the system rapidly (and irreversibly) into the biphasic region (Figure 2).

Neutron Scattering. (i) To characterize the static structures of the CPCl/hexanol/dextrose/heavy brine samples, standard SANS measurements on samples in Helma Suprasil quartz "banjo" cells were performed both on the NG-3 SANS spectrometer[40] at the Cold Neutron Research Facility, National Institute of Standards and Technology, Gaithersburg, and on the High Flux Isotope Reactor SANS instrument at Oak Ridge National Laboratory.[41] The incident neutron wavelength used was 6 Å with $\Delta\lambda/\lambda \sim 0.15$ at NIST and 4.75 Å with $\Delta\lambda/\lambda \sim 0.05$ at the HFIR. The scattering data were collected on a two-dimensional detector and covered the entire accessible Q range or roughly 0.003−0.4 Å^{-1}. Each raw data set was corrected for detector background, sensitivity, and scattering from the empty cell in the usual fashion.[42] Conversion to the absolute scale on NG-3 is done in the standard manner using the direct beam as a primary standard and correcting for sample transmission. At the HFIR, the absolute scale is obtained by comparison with precalibrated secondary standards based on measurement of the beam flux, the vanadium incoherent cross section, and the scattering from water.[42] All 2D data in these measurements were isotropic and were radially averaged.

(ii) SANS under shear measurements were performed on the NG-3 SANS spectrometer, and the incident neutron wavelength used was 6 Å with $\Delta\lambda/\lambda$ of 15%. The scattering data were collected on a two-dimensional detector covering a range of momentum transfers Q from 0.004 to 0.03 Å^{-1}. Samples were Couette sheared between two concentric quartz cylinders with an annular gap of 0.5 or 1 mm (outer radius 25 mm) with the inner stator cylinder stationary and maintained at constant temperature (20 ± 0.1 °C) to control viscous heating. All measurements were performed below the critical Reynolds number for this configuration ($\sim$1500). Our ORNL neutron Couette cell has a specially designed vapor barrier to absolutely minimize the effects of evaporation. This is critical in obtaining consistent reproducible results in a very sensitive system such as the L_3 sponge phase studied here, which, as noted above, only a very small amount of cosurfactant evaporation will bring into an equilibrium L_α lamellar phase.[43]

The two scattering configurations used in the Couette SANS measurements are shown in Figure 3a: In the radial geometry, the neutron beam passes through the sample along the velocity gradient direction, ∇V, across the diameter of the cylinders, while, in the tangential geometry, the beam passes along the flow direction, V, along the tangent of the sample annulus. These configurations allow us to measure membrane orientations relative to the (V, Z) and (∇V, Z) planes, respectively, where Z denotes the rotation axis of the cylinders, which in this case is the vorticity axis of the shear field. Thus, in Figure 3b we show schematics of the pattern of Bragg peaks expected in scattering from the a, b, and c orientations of an aligned lamellar phase under Couette shear. A typical measuring time was 5 min for the radial geometry and 25 min for the tangential geometry. In the radial configuration, a 10 mm diameter sample aperture was used, while, in the tangential one, rectangular slits 12 mm high and with widths of 0.6 and 0.4 mm were used for the 1 or 0.5 mm gaps, respectively.

Each raw data set was corrected for detector background, sensitivity, and scattering from the empty cell in the usual fashion.[42] In the radial scattering configuration, conversion to an absolute scale can be done in the standard manner using the direct beam as a primary standard, correcting for sample transmission and thickness, $t_{RAD} = 2g$ (i.e. twice the Couette gap). Absolute calibration in the tangential geometry is more problematic and is usually accomplished (if indeed it is done at all) by matching the intensity of an isotropic scatterer in the radial geometry with it in the tangential one. In this work we used an alternate method: from the tangential transmission T_{TAN} we obtain an effective tangential thickness t_{TAN} consistent with the absorption coefficient obtained from the radial transmission T_{RAD} and its known thickness t_{RAD}, that is, $t_{TAN} = t_{RAD} \ln[T_{TAN}]/\ln[T_{RAD}]$. Using this value then allows reduction of the tangential data to an absolute scale in the same manner as is described above for the radial data. This method provides good quantitative agreement between these configurations for these samples. It is fully described in a previous

(39) Chen, V. Ph.D. Thesis, University of Minnesota, 1988.

(40) Glinka, C. J.; Barker, J. G.; Hammouda, B.; Krueger, S.; Moyer, J. J.; Orts, W. J. *J. Appl. Crystallogr.* **1998**, *31*, 430.

(41) This instrument has been shortened from the 30 m geometry described in detail by: Koehler, W. C. *Physica B* **1996,** *137*, 320. The sample to detector distance is now 12 m (down from 18 m).

(42) Wignall, G. D.; Bates, F. S. *J. Appl. Crystallogr.* **1986**, *20*, 28.

(43) Porcar, L.; Hamilton, W. A.; Butler, P. D.; Warr, G. G. *Rev. Sci. Instrum.* **2002**, *73*, 2345.

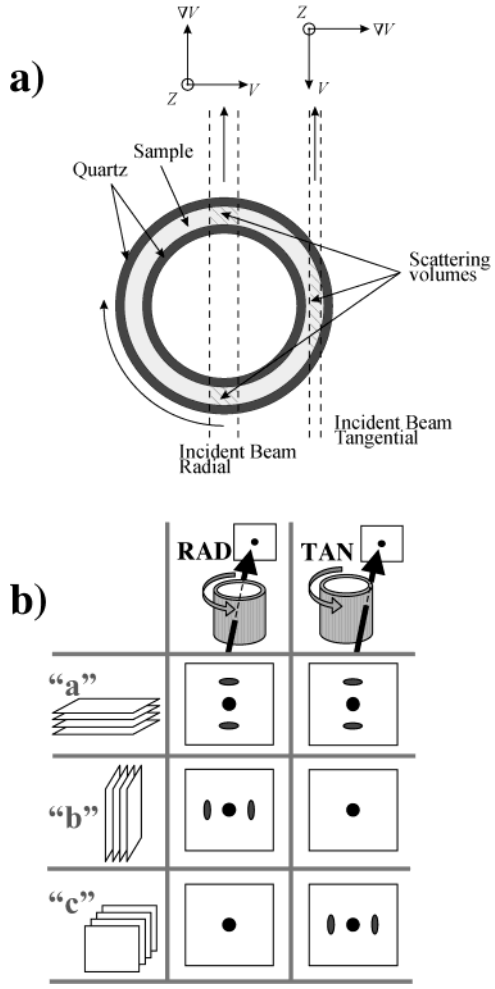

Figure 3. (a) Schematic representation of the sample geometry in a Couette shear cell neutron scattering experiment for radial and tangential geometries and identification of the axes with respect to the shear cell. (b) Schematic of expected scattering peaks in radial and tangential geometries from aligned lamellar phases in the Couette shear field with the following membrane orientations: a, perpendicular to the flow vorticity direction *Z*; b, perpendicular to the flow direction *V*; c, perpendicular to the shear gradient ∇*V*.

paper,[43] which also gives details of the design and capabilities of the ORNL Couette cell.

Rheology. The rheological characterizations of CPCl/hexanol/dextrose/heavy brine samples were carried out using a RheoStress 150 rheometer from Haake (Gebr. Haake GmbH, Karlsruhe, Germany). The measurements were performed at controlled Couette shear rates using a coaxial cylinder stress sensor of double gap geometry (Haake DG41) designed for low viscosity measurements. The gap widths were 0.3 and 0.25 mm. The cup of the coaxial cylinders is constructed of stainless steel, while the rotating stress sensor bob is titanium plated. For our samples, this apparatus allows viscosity measurement at shear rates sufficiently low to obtain the zero shear rate limit viscosity and high enough to reach the non-Newtonian range. Rheological measurements were taken by shear sweeping over a range of $\dot{\gamma}$ from 1 to 8000 s^{-1}, waiting at each discrete shear rate for a steady shear response to be established, at a fixed temperature of 20 °C with samples free of foam. A full vapor barrier is not available for this instrument, and a makeshift installation was only partially effective so each measurement was limited to about a 20 min duration. Afterward the recovered samples were sealed in small bottles and carefully observed between crossed polarizers to ensure that they still showed the isotropic sponge structure and exhibited no static birefringence indicating the presence of an equilibrium lamellar phase component, which as the phase diagrams (Figure 2) of this system indicate, can arise relatively rapidly in this unsealed sample bob upon the evaporation of only a small amount of the hexanol cosurfactant.[36]

Dynamic Light Scattering (DLS). The simple quasi-elastic light scattering determinations of the membrane's cooperative diffusion coefficient presented here were taken at a single scattering angle of 90° using a Coulter model N4 MD "submicron particle analyzer" (Coulter Electronics, Inc., Hialeah, FL) at the He/Ne laser wavelength $\lambda = 6328$ Å. Values were corrected for refractive index variation of the samples from 1.34 for the normal brine solvent to 1.42 at the highest dextrose concentration, $\psi = 0.4$.

Experimental Results

Equilibrium Phase Behavior of Sweetened Membrane Phases. At volume fractions up to $\psi = 0.4$ (the highest concentration used in these measurements), the presence of dextrose in the brine solvent (0.2 M NaCl) was not observed to alter the sequences of phases in this system. Simple visual and crossed polarizer observations showed that changing the mass ratio *h* of the membrane constituents hexanol and CPCl, which controls the interfacial film curvature, gives rise to micelle, lamellar, and sponge phases and coexistence regions in the same sequence as that encountered in the unsweetened CPCl/hexanol/brine system. There were relatively small shifts in the observed phase boundaries. Figure 2 represents the phase diagram in the region of the stability domain of the sponge phase for the CPCl/hexanol membrane system (a) in H_2O brine and (b) in fully sweetened H_2O brine ($\psi = 0.4$). The stability region of the sponge phase is of about the same width with respect to *h* over the range of membrane volume fractions, but as ψ changes from 0 to 0.4, the value of *h* at which the sponge phase occurs decreases by about 12%. Substitution of heavy D_2O brine as a constituent of the system for neutron contrast in the scattering measurements also results in a small shift in the phase region, lowering *h* by about 2% for systems with and without dextrose. Again, the phase sequence is unchanged, and we found that phase widths in *h* were the same as those for the corresponding undeuterated system.

Static Structure of Sweetened Sponge Phases. We have investigated the effect of dextrose on the convoluted sponge phase structure using SANS on the deuterated sponge system. Figure 4a represents fits to the measured SANS intensity for sponge samples at a constant membrane volume fraction $\phi = 0.15$ for normal heavy brine ($\psi = 0$) and at the dextrose solvent volume fractions used in this study: $\psi = 0.1$, 0.2, 0.3, and 0.4. Clearly, the overall scattering pattern and the position and width of the correlation peak characteristic of the sponge pore size appear to be in good agreement, indicating that the structure is unaffected by the addition of dextrose.

Quantitative values were obtained from the following fit to the data. We have used the SANS structure factor due to Lei et al.,[44] which may be written

$$S(Q) = 1 + \frac{A \arctan[Q\zeta_{io}/2]}{Q} + \frac{B}{1/\xi_3^{\,2} + (Q - Q_3)^2} \quad (1)$$

The first two terms of this expression are the structure factor derived by Roux et al.,[45,46] which describes the membrane correlations on a length scale much larger than the pore size in terms of an "inside−outside" correlation length ζ_{io}. This expression has successfully been used to

(44) Lei, N.; Safinya, C. R.; Roux, D.; Liang, K. S. *Phys. Rev. E* **1997**, *56*, 608.
(45) Roux, D.; Cates, M. E.; Olsson, U.; Ball, R. C.; Nallet, F.; Bellocq, A. M. *Europhys. Lett.* **1990**, *11*, 229.
(46) Roux, D.; Coulon, C. *J. Phys. Chem.* **1992**, *96*, 4147.

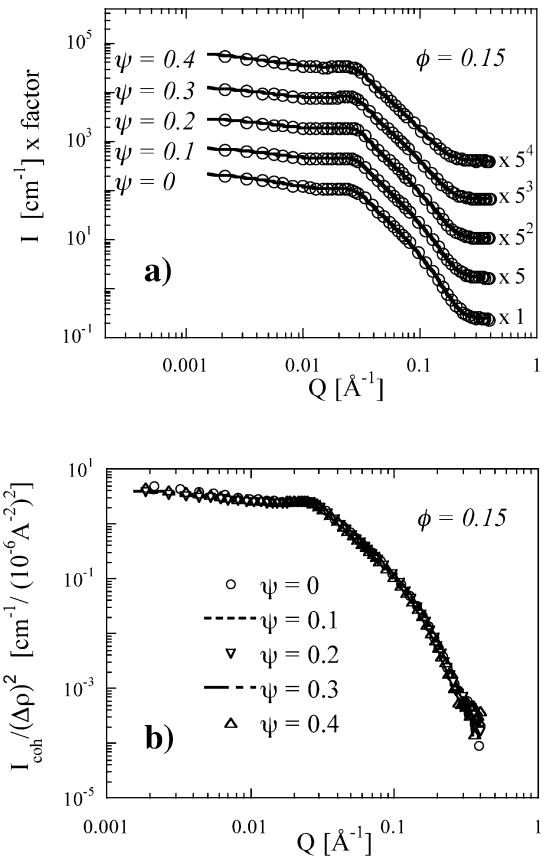

Figure 4. (a) Measured SANS intensity and best fits from eqs 1 and 2 with parameters from Table 1 for sponge phases at constant membrane volume fraction $\phi = 0.15$ for a range of dextrose volume fractions. The absolutely scaled intensity curves are shifted for clarity. (b) Normalized coherent SANS intensity $I_{coh}/(\Delta\rho)^2$ for these samples, where $\Delta\rho$ is the neutron contrast between the hydrophobic membrane tail and the solvent. For the $\psi = 0$ sample $\Delta\rho = 6.42 \times 10^{-6}$ Å^{-2} and for the $\psi = 0.4$ sample $\Delta\rho = 4.47 \times 10^{-6}$ Å^{-2}, so the normalizing factor $(\Delta\rho)^2$ varies by about 2 over the range of this series.

fit light scattering data from different systems over a broad range of very small Q. The choice of a volume fraction $\phi = 0.15$ for this dextrose series allows us to measure the scattering over a Q range where it is dominated by the contribution of the final Lorentzian term, which characterizes the scattering from the sponge structure by a correlation length ζ_3 and the average pore size $\xi \equiv 2\pi/Q_3$. The concentration is high enough that the contribution of the larger scale structure in our fits is that of a simple small A/Q term, while it is low enough that form factor scattering variations due to the membrane's scattering contrast thickness are also relatively smooth near the sponge correlation peak.

For the form factor, Lei et al.[44] used a numerical calculation of the scattering randomly oriented disks of the membrane with a definite radius R and contrast thickness t_0—in this case the thickness of the membrane's hydrocarbon core. We have used the form factor for scattering from membrane "discoids" of contrast thickness t_0 with a Gaussian distribution of transverse scattering length density characterized by a radius of gyration σ. For the purposes of fitting our sponge scattering data, the form factors of disks and discoids should be essentially equivalent when their radii of gyration are the same, that is, when $R = \sqrt{2}\sigma$, with the latter having the advantage of being more mathematically tractable. Starting from an averaged membrane form factor due to Nallet et al.,[47] we

Table 1. Sponge Structure Parameters Obtained for the Fits Shown in Figure 4a to the Small Angle Neutron Scattering Signal from $\phi = 0.15$ Sponge Phase Samples at a Series of Dextrose Volume Fractions in Brine ψ

ψ	ζ_3 (Å)	$\xi \equiv 2\pi/Q_3$ (Å)	σ (Å)	t_0 (Å)	I_{incoh} (cm^{-1})
0	81	240	25.1	20.4	0.23
0.10	87	236	26.7	20.7	0.32
0.20	89	234	27.6	20.8	0.41
0.30	90	236	27.8	20.9	0.53
0.40	86	240	26.9	20.7	0.63

have derived an analytical approximation for the form factor of these discoids averaged over random orientations:

$$P(Q) \approx 4(\pi\sigma^2\Delta\rho)^2 \frac{(1 - \cos[Qt_0]\exp[-Q^2t_0^2/32])/Q^2}{Q^2\sigma^2 + 2\exp[-Q^2\sigma^2/6]} \quad (2)$$

This form is simplified slightly from a previously published approximate form[26] in that it assumes that (as is the case for the dilute and semidilute samples studied here) the neutron contrast discoids have relatively large transverse radii of gyration σ, which we may therefore use to approximate their full radius of gyration $R_g \cong (\sigma^2 + t_0^2/12)^{1/2}$; that is, we assume the transverse radius of gyration is much greater than the rms width of the hydrocarbon core $\sigma \gg t_0/(12)^{1/2}$. As expected, this expression agreed well with the numerically calculated values of the Lei et al. form factor when $R = \sqrt{2}\sigma$; however, the availability of an analytical form factor makes fitting the scattering data simpler and much faster. Each such discoid has an effective scattering contrast volume $V_D = \pi\sigma^2 t_0$. (Thus, at low Q we may readily verify that this form factor approximately recovers the expected Guinier behavior, $P(Q\rightarrow 0) \approx (\Delta\rho)^2 V_D^2 \exp[-Q^2\sigma^2/3]$.)

The observed scattering intensity $I_{coh}(Q)$ is then the sum of the coherent structural scattering $I_{coh}(Q) = NS(Q)P(Q)$, where N is the effective number density of the discoids in solution, and an isotropic incoherent contribution I_{incoh} dominated by hydrogen scattering.

The effective number density of these discoids in solution is determined from their full volume; that is, $N = \phi/\pi\sigma^2\delta$, where δ is the full membrane thickness as opposed to the scattering contrast thickness t_0. The charged surface group layers on the outer surfaces of CPCl/hexanol membranes are about 2.5 Å thick and have lower contrast with respect to the solvent both intrinsically and because of penetration of solvent molecules which are excluded from the hydrophobic core. In the following fits, we therefore maintained $\delta \equiv t_0 + 5$ Å.

The values of the structural parameters obtained from the fits to these data are presented in Table 1. None of the fit parameters, even those most sensitive to change of the sponge structure, the pore size ξ and the sponge correlation length ζ_3, vary systematically or significantly with the sugar concentration. This is further illustrated in Figure 4b, which shows the coherent scattering intensity from these samples after subtraction of the incoherent scattering background obtained from the fits and scaling out the expected differences in scattering power between the samples (which varies by about a factor of 2 over the series).

(47) Nallet, F.; Laversanne, R.; Roux, D. *J. Phys. II* **1993**, *3*, 487. The starting lamellar form factor may be viewed as arising from averaging a standard lamellar form factor over a Gaussian distribution of membrane thicknesses. The specific parameters in the exponential term $\exp[-Q^2 t_0^2/32]$ in the numerator of eq 2 correspond to this distribution having a standard deviation equal to one-quarter the contrast thickness, a value which both we and Nallet et al. found satisfactory. Note: An obvious typographical error in our published derivation of the random orientation discoid form factor in ref 26 omitted the minus sign in the exponential in this equation (there equation C2).

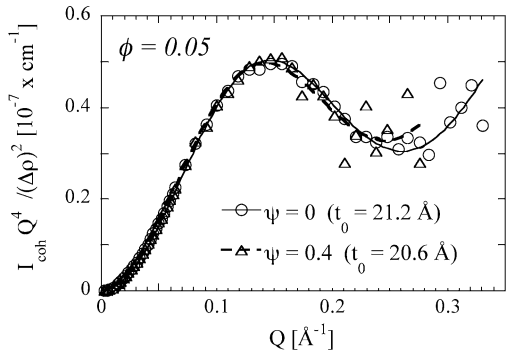

Figure 5. Higher Q range scattering measurements on two samples at membrane volume fraction $\phi = 0.05$ in normal brine and at our highest dextrose volume fraction of $\psi = 0.4$. Intensities have been scaled by $Q^4/(\Delta\rho)^2$. Fits are to the isotropically averaged discoids form factor eq 3.

If we assume there is no incorporation of dextrose into the membrane, the scattering power will be proportional to the square of the difference in scattering length density of the CPCl/hexanol hydrophobic core and the dextrose in heavy brine solvent for that particular sample. Thus scaled, the scattering data from all five samples are in excellent agreement, indicating that the dextrose is excluded from the membrane and has no significant effect on the sponge structure over these length scales.

The hydrocarbon core thickness obtained from the fits in Figure 4a is $t_0 = 20.7 \pm 0.2$ Å, which compares extremely well with previous determinations of the CPCl/hexanol membrane contrast width, $t_0 = 20.5 \pm 1$ Å, obtained in scattering experiments on sponge and lamellar membrane phases in normal brine.[26,48,49] As those measurements focus on the sponge phases's characteristic correlation pore peak scattering, we chose a relatively high membrane volume fraction to ensure that this appeared at higher Q to separate it from the strong long-range correlation scattering at low Q. Figure 5 shows higher Q range measurements on two samples at lower membrane volume fraction $\phi = 0.05$ in normal brine and at our highest dextrose volume fraction of $\psi = 0.4$. At this choice of concentration and higher Q range ($Q\sigma \gg 1$), the scattering is dominated by the membrane form factor ($S(Q) \cong 1$) and may be approximated by[50]

$$I(Q) \approx NP(Q) \approx \frac{4\pi\phi(\Delta\rho)^2}{\delta} \frac{(1 - \cos[Qt_0] \exp[-Q^2 t_0^2/32])}{Q^4} \quad (3)$$

In the presentation of this scattering data, we have scaled out both the strong Q^{-4} dependence in this range and the nominal scattering contrast factor $(\Delta\rho)^2$. We note that both the magnitude and functional form of the result $I(Q)Q^4/(\Delta\rho)^2$ depend directly on the membrane thicknesses $\delta \equiv t_0 + 5$ Å. Clearly, over their common range, the rescaled scattering measurements are in excellent agreement. (The usable signal-to-noise ratio for the unsweetened brine sample data extends to higher Q, since it has both a stronger coherent scattering signal due to higher membrane to solvent contrast and a lower contribution to the incoherent background scattering from the solvent.) Again, the fits to these data give values of t_0 consistent with each other and with earlier determinations of the hydrocarbon core thickness of the CPCl/hexanol membrane.

To first-order, the scale invariance of the curvature elasticity of membrane phases such as the sponge scale leads to a simple scaling of the structure factor scattering.[51,52] The scattered intensity is inversely proportional to the membrane volume fraction ϕ, as are the sizes of such features as the pores. The latter means that the positions of such features as the pore−pore correlation peak in Q are proportional to ϕ. To the extent that this scaling may be energetically driven, it is important to verify that it is maintained for the high dextrose concentration, low membrane volume fraction samples required for the rheological measurements presented here. Figure 6 shows static scattering measurements before (a) and after (b) rescaling to eliminate both scale invariance and scattering power ($I\phi/(\Delta\rho)^2$ vs Q/ϕ) for two dilute heavy brine sponge structural series: (i) a series at a constant membrane volume fraction of $\phi = 0.05$, with varying dextrose concentrations in the brine $\psi = 0$, 0.2, 0.3 and 0.4, and (ii) an (intersecting) series with a constant high dextrose volume fraction $\psi = 0.4$ with varying membrane volume fractions $\phi = 0.03$, 0.05, 0.07, and 0.10. The identity of the rescaled profiles is striking, and the scale invariance of the sponge structure is clearly maintained even at the highest ratio of dextrose to CPCl/hexanol in these samples.

Rheology: *(a) Low Shear Rate Response.* The response of a complex fluid to shear may be described in terms of the Peclet number or, equivalently, in terms of the Deborah number[2] $De \equiv \dot{\gamma}/\omega$, defined as the ratio of the applied shear rate to the characteristic response frequency ω of the material. (In our case, a simple estimate of the response frequency can be inferred from the expression for the critical shear rate derived from the Peclet number $\omega \sim \dot{\gamma}_c \sim k_B T/\xi^3\eta_s$, yielding $Pe \sim De \sim \dot{\gamma}\xi^3\eta_s/k_B T$.) For $De < 1$, the response is essentially Newtonian, and in this section, we compare the rheological properties of sweetened and unsweetened sponges in this limit, which holds for all our samples for shear rates $\dot{\gamma} \leq 100$ s^{-1}. (See, for instance, the samples's viscosity in the low shear region of Figures 9 and 12a.). Although we note a definite increase of the viscosity for dextrose-containing samples compared with those measured with the normal brine system, this Newtonian behavior indicates that shear has no significant influence on the sponge microstructure of any of these samples in this range.

Snabre and Porte[53] proposed a stress relaxation mechanism to describe the viscosity behavior of the sponge phase at low shear rates at which the morphology is only stretched, that is, if the sponge structure is not entangled or passages between membranes are destroyed. Relief of stresses in the slightly distorted sponge structure does not therefore depend on complicated high energy processes, such as passages moving past or across each other or being created or destroyed, but is dominated by simple viscous flow of the surfactant in the membrane and the solvent through the passages. In this case, they predicted

(48) Bouglet, G.; Ligoure, C. *Eur. Phys. J. B* **1999**, *9*, 137.

(49) Roux, D.; Nallet, F.; Freyssingeas, E.; Porte, G.; Bassereau, P.; Skouri, M.; Marignan, J. *Europhys. Lett.* **1992**, *17*, 575.

(50) The validity of eq 3 at high Q may be further confirmed by comparing its behavior to that of the expected Porod form for scattering from randomly oriented sharp interfaces in this limit; that is, $I(Q) \approx 2\pi(\Delta\rho)^2 S_v/Q^4$, where S_v is the total interfacial area per unit volume (Porod, G. *Kolloid Z.* **1951**, *124*, 82). A two sided patch of membrane has the interfacial area $2A$ and volume $A\delta$, which is a fraction ϕ of the total volume occupied (on average) by the patch; so $S_v = (2A)/(A\delta/\phi) = 2\phi/\delta$. Inserting this in the Porod expression, we recover the large Q limit of eq 3: $I(Q) \gg 4\pi\phi(\Delta\rho)^2/\delta Q^4$.

(51) Skouri, M.; Marignan, J.; Appell, J.; Porte, G. *J. Phys. II* **1991**, *1*, 1121.

(52) Porte, G. From Giant Membranes to Fluid Membranes: Polymorphism in Dilute Solutions of Surfactant Molecules. In *Soft Matter Physics*; Daoud, M., Williams, C. E., Eds.; Springer: Berlin, 1995; Chapter 5, p 155.

(53) Snabre, P.; Porte, G. *Europhys. Lett.* **1990**, *13*, 641.

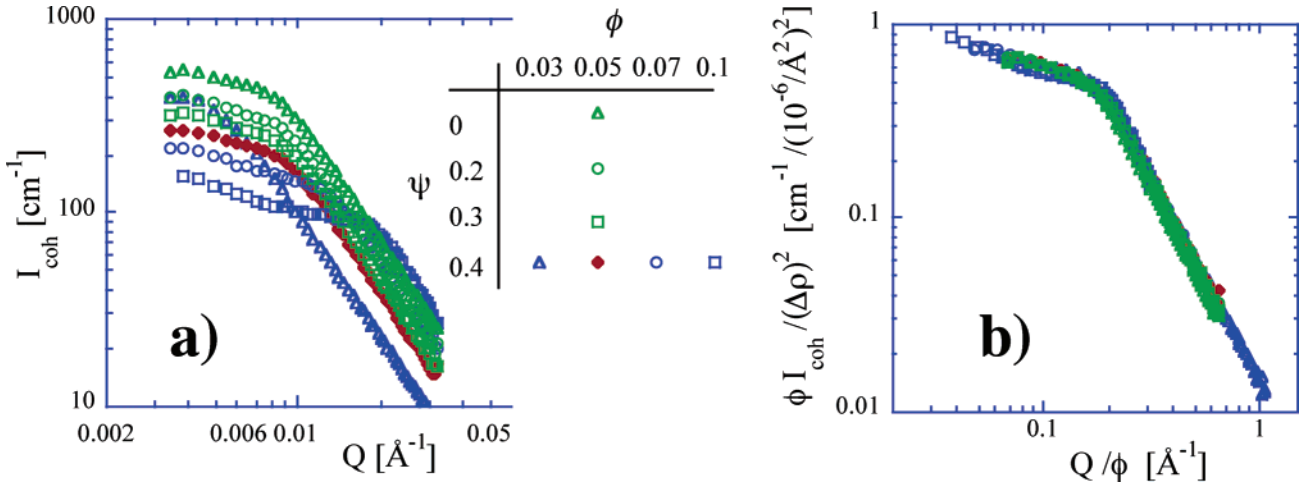

Figure 6. Static scattering measurements before (a) and after (b) rescaling to eliminate both scale invariance and scattering power ($I\phi/(\Delta\rho)^2$ vs Q/ϕ) for two dilute heavy brine sponge sample series: at a constant membrane volume fraction of $\phi = 0.05$, with varying dextrose concentrations in the brine $\psi = 0$, 0.2, 0.3, and 0.4; and at a constant dextrose volume fraction $\psi = 0.4$, with varying membrane volume fractions $\phi = 0.03$, 0.05, 0.07, and 0.10.

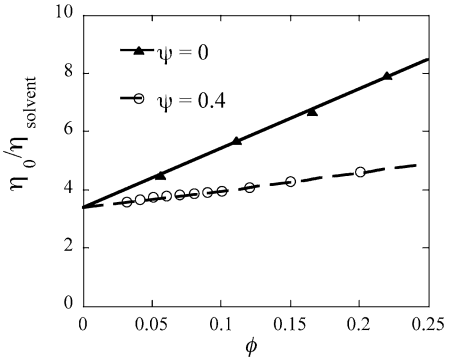

Figure 7. Variation of η_0/η_s, the ratio of the low shear rate viscosity of sponge phases η_0 to the solvent viscosity η_s, with membrane volume fraction ϕ, for normal brine solvent ($\eta_s = 1.0$ cP) and viscosity highest dextrose volume fraction of $\psi = 0.4$ brine ($\eta_s = 13.4$ cP).

that the low shear viscosity of sponge phases should depend on membrane volume fraction as $\eta_0(\phi) = A\eta_s + B\phi$. Here the prefactor A directly represents the apparent viscosity change due to flow pattern restrictions imposed upon the solvent by the scale invariant sponge geometry. As such, it should therefore be independent of the chemical system and membrane volume fraction. Snabre and Porte[53] and later Gomati et al.[54] found values of A of about 3 for CPCl/hexanol in normal brine sponges. The second term takes into account chemical system and membrane volume fraction dependent effects such as the diffusion of surfactant molecules within the membrane and surface area drag as the solvent moves past it.

Figure 7 shows the variation in the ratio of the zero shear limit viscosity of sponge samples to that of the solvent η_0/η_s for a series of membrane volume fractions ϕ without dextrose $\psi = 0$ and at high dextrose volume fractions $\psi = 0.4$. The measured viscosity for our light water brine at 20 °C was 1.04 cP, while that of the high dextrose brine is more than an order of magnitude higher, 13.4 cP. For both sample series the predicted linear behavior with membrane volume fraction is observed with the sponge to solvent viscosity ratio extrapolating to almost exactly the same value, $A \approx 3.4$ at $\phi = 0$, indicating that the geometry dependent prefactor is the same for this system with and without dextrose added to the brine.

(54) Gomati, R.; Bouguerra, N.; Gharbi, A. *Physica B* **2002**, *322*, 262.

Cooperative Membrane Diffusion Coefficient. Porte et al.[55] have demonstrated that for symmetric sponge[56] phases the characteristic relaxation frequency of concentration fluctuations τ_D^{-1} determined by dynamic light scattering (DLS) is simply related to Q^2, with the constant of proportionality being the cooperative membrane diffusion coefficient $\tau_D^{-1} = DQ^2$. This is consistent with a simple diffusion process under the constraint of the conservation of the membrane volume fraction in these systems. Using the classical Stokes−Einstein relation for objects of effective hydrodynamic radius ξ_H, we may therefore write $D = k_BT/6\pi\eta_s\xi_H$. Figure 8a shows measurements D as determined by DLS for sponge samples at a constant membrane volume fraction $\phi = 0.05$ for our full range of dextrose volume fractions $\psi = 0-0.4$ plotted against the reciprocal of the viscosity of the brine solvent, $1/\eta_s$. Clearly, the measured membrane diffusion coefficients are inversely proportional to the solvent viscosity. From the straight line fit to these data we may infer an effective hydrodynamic radius of ξ_H of 760 Å, which, as we might expect, is roughly equal to the pore−pore correlation distance $\xi \approx 800$ Å ($Q_3 = 0.008$ Å^{-1}) measured for corresponding $\phi = 0.05$ sponge samples in sweetened heavy brine. The measured viscosities for the light and heavy brines with added dextrose solvent used in the measurements presented in this paper are plotted in Figure 8b.

(b) Full Shear Response. We have found the slower response times in this system due to the increase in the solvent viscosity with the addition of dextrose to the brine make it relatively easy to reach Deborah numbers *De* above unity at experimentally convenient shear rates, viscosities, and membrane volume fractions. Figure 9 shows that, while a normal brine sponge sample at a membrane volume fraction $\phi = 0.1$ is Newtonian, indicating that $De \leq 1$ to the highest shear rate accessible in our Couette rheometer, $\dot{\gamma} \sim 8000$ s^{-1}, a highly sweetened sponge ($\psi =$

(55) Porte, G.; Delsanti, M.; Billard, I.; Skouri, M.; Appell, J.; Marignan, J.; Debeauvais, F. *J. Phys. II* **1991**, *1*, 1101.

(56) This simple proportionality of the relaxation frequency to Q^2 cannot be assumed for asymmetric sponges (Granek, R.; Cates, M. E. *Phys. Rev. A* **1992**, *46*, 3319) or hyperswollen sponge phases (Freyssingeas, E.; Roux, D.; Nallet, F. *J. Phys. II* **1997**, *7*, 913). However, both of these exceptions apply to much higher dilution than any considered in this work. Further, it has been shown[19] that the CPCl/hexanol/brine system does not in fact exhibit any of these peculiarities, and we may expect this to hold for our dextrose modification of the solvent of this system.

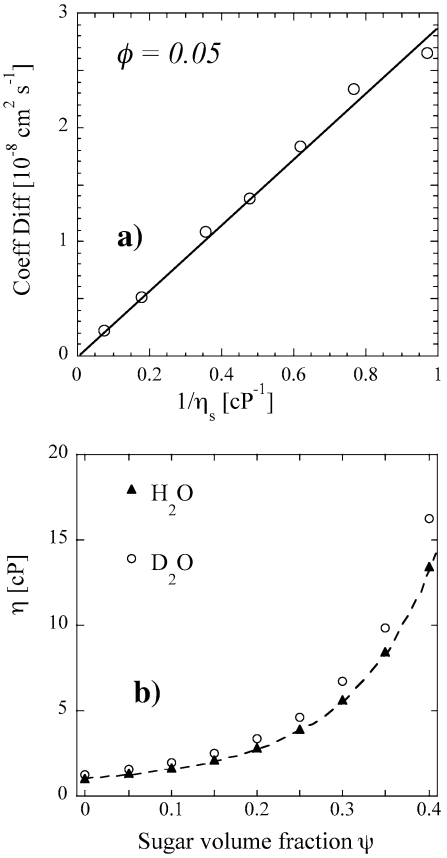

Figure 8. (a) Cooperative coefficient of diffusion D for sponge samples at a constant membrane volume fraction $\phi = 0.05$ for our full range of dextrose volume fractions $\psi = 0-0.4$ plotted against the reciprocal of the viscosity of the brine solvent, $1/\eta_s$. (b) Viscosity η_s versus dextrose volume fraction ψ for the normal and heavy brine solvents used in this study. The dashed line shows *CRC Handbook of Chemistry and Physics* data.

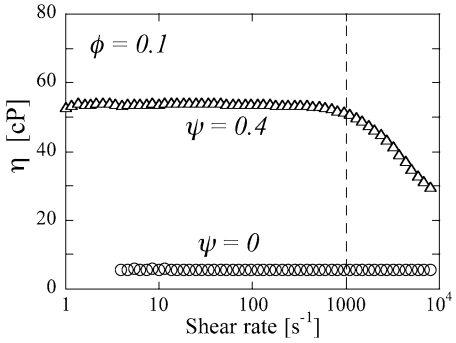

Figure 9. Viscosity η versus shear rate $\dot{\gamma}$ for CPCl/hexanol membrane sponge samples with membrane volume fraction $\phi = 0.1$ in normal brine solvent ($\psi = 0$) and at dextrose volume fraction in brine $\psi = 0.4$. While the normal brine sponge sample is Newtonian to shear rates of at least 8000 s^{-1}, the $\psi = 0.4$ sponge shows pronounced shear thinning above ~500 s^{-1}.

0.4) at the same volume fraction begins to shear thin at a shear rate over an order of magnitude lower. This is consistent with the scaling relation outlined above, which predicts that critical shear rates in this system should scale inversely with the solvent viscosity.

The full range of viscosity versus shear rate behavior we observed for these sweetened sponge systems is accessible in our rheometer at a lower membrane volume fraction of $\phi = 0.05$ at the same high dextrose concentration $\psi = 0.4$ and is shown in Figure 10a. Again, this is consistent with the scaling predictions which indicate that halving the membrane volume fraction should reduce critical shear

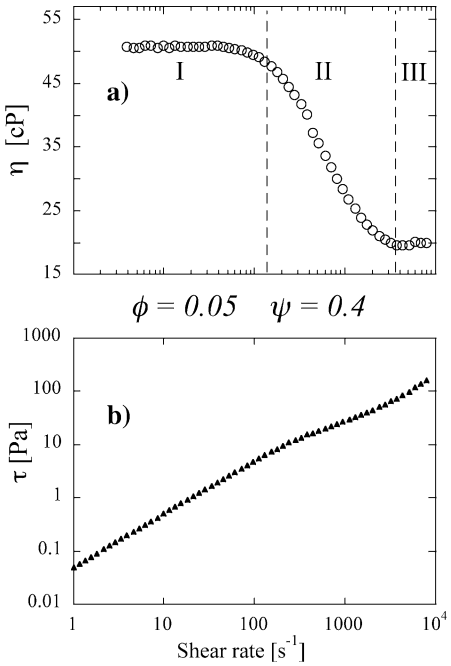

Figure 10. Full range of shear response observed for these sweetened sponge systems in (a) viscosity η and (b) shear stress τ versus $\dot{\gamma}$ for a membrane volume fraction of $\phi = 0.05$ at high dextrose concentration, $\psi = 0.4$.

rates by a factor of 8. The full shear behavior is characterized by three distinct regions: At low shear rates (region I), the sponge phase sample exhibits Newtonian behavior (as described in the previous section), and its structure is apparently not affected by the shear. In an intermediate range (region II), the solution shear thins, indicating that some structural change is occurring. At higher shear rates for our lower membrane volume fraction, high solvent viscosity samples, we now reach a third "quasi-Newtonian" region (III), where the viscosity is nearly constant once again. Figure 10b shows the shear stress measurements from which the viscosity is derived ($\tau = \eta\dot{\gamma}$). The absence of a plateau in this stress curve or of any detectable hysteresis[57] in region II indicates that the structural change which gives rise to the shear thinning is not first-order as predicted by the theory of Cates and Milner[28] and rules out biphasic effects such as "shear banding",[58,59] distinguishing this response from those recently reported for polymeric bicontinuous microemulsions by Krishnan et al.[60] The gradual variation of the viscosity over the shear-thinning region for this system suggests a transformation that proceeds by progressively distorting the membrane structure rather than creating a new phase.

SANS Measurements of Sweetened Sponge Phases under Shear. The details of the microstructural responses of sweetened sponge phases to shear were investigated in a series of Couette SANS measurements on a CPCl/hexanol/heavy brine/dextrose sponge phases. Figure 11

(57) No hysteresis in the viscosity was detectable in measurement scans sweeping the shear rate up or down within region II. Nor did we observe any difference in the viscosity measured in this region after shearing for 10 s or 5 min at a particular shear rate.

(58) Berret, J. F.; Roux, D. C.; Lindner, P. *Eur. Phys. J. B* **1998**, *5*, 67.

(59) Olmsted, P. D.; Lu, C. Y. D. *Phys. Rev. E* **1997**, *56*, R55.

(60) Krishnan, K.; Almdal, K.; Burghardt, W. R.; Lodge, T. P.; Bates, F. S. *Phys. Rev. Lett.* **2001**, *87*, 098301. Krishnan, K.; Chapman, B.; Bates, F. S.; Lodge, T. P.; Almdal, K.; Burghardt, W. R. *J. Rheol.* **2002**, *46*, 529. This work presents an excellent example of constant shear stress measurements corresponding to a "flow-induced phase separation" (i.e. biphasic) regime expected for a first-order transition.

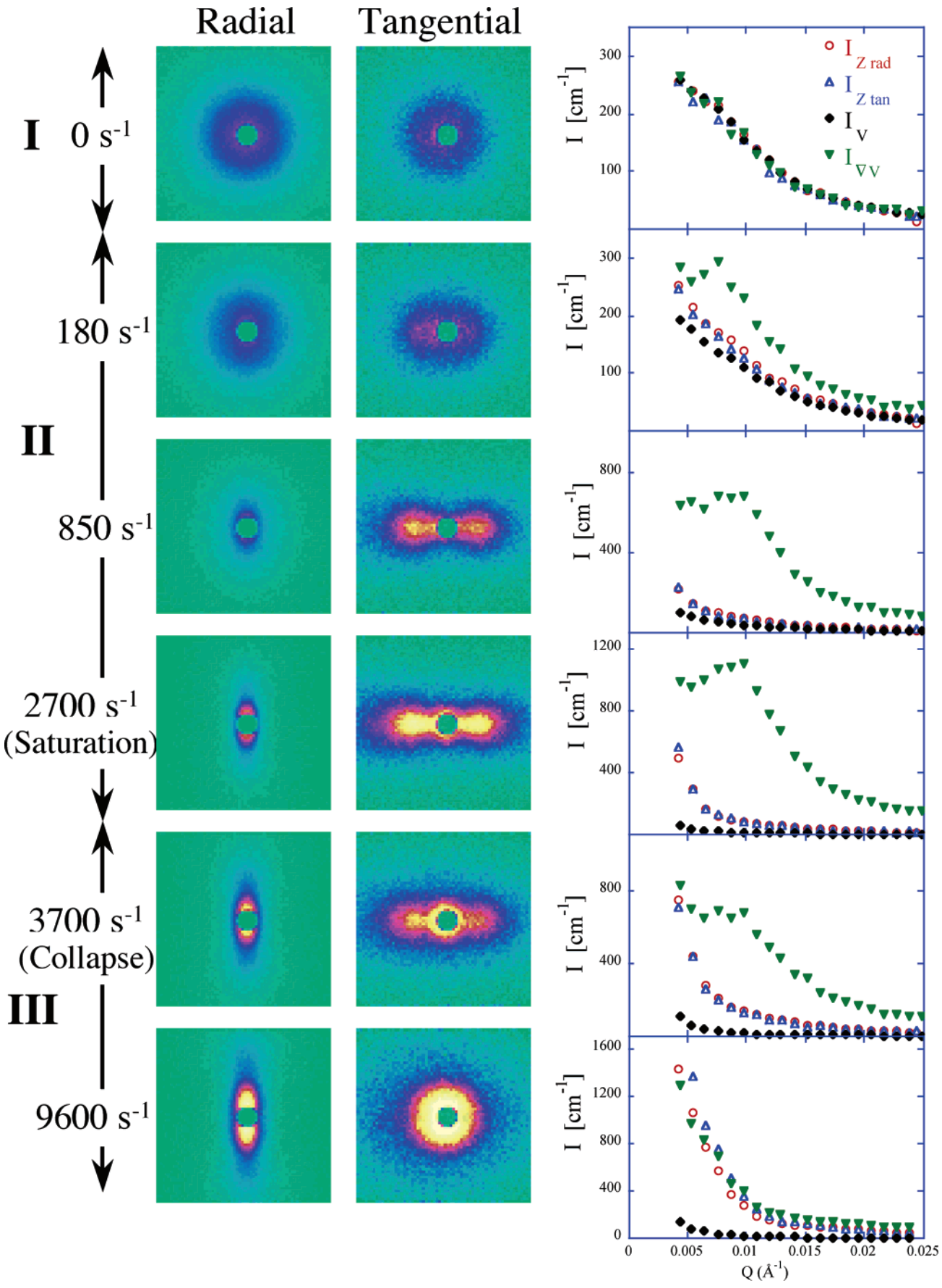

Figure 11. Variation in scattering in radial and tangential geometries with shear $\dot{\gamma}$ for a $\phi = 0.05/\psi = 0.4$ heavy brine sponge sample phase in radial and tangential geometries for a range of shear rates spanning all three shear regions. The graphs on the right show the corresponding scattering intensity of these data along the flow (V), shear gradient (∇V), and vorticity (Z) axes, as identified in Figure 3 for the two geometries: $I_{Z(RAD)}$ and I_V for the radial configuration; $I_{Z(TAN)}$ and $I_{\nabla V}$ for the tangential configuration. Each intensity has been sector averaged over $\Delta\theta = \pm 10°$ of the axis.

represents the scattering patterns obtained under shear from a $\phi = 0.05$, high dextrose concentration $\psi = 0.4$ sponge sample in both radial and tangential geometries (Figure 3a). This corresponds closely to the light water sponge phase sample with the rheological response presented in Figure 10. The viscosity of heavy brine at $\psi = 0.4$ was measured to be 16.2 cP compared with 13.4 cP for light brine. Static and very low shear rate ($\dot{\gamma} \leq 100$ s^{-1}) scattering patterns in both geometries show the broad isotropic ring characteristic of sponge phase structures. This region corresponds to the Newtonian region I for the light brine sample. As the shear rate increases further (100 s^{-1} $\leq \dot{\gamma} \leq$ 2000 s^{-1}), corresponding to the shear-thinning region II, the scattering patterns become strongly anisotropic. In the radial geometry, the overall scattering intensity in the patterns decreases, but somewhat more rapidly in the flow velocity direction (V) than in the vorticity direction (Z). These radial geometry observations are at low shear consistent with earlier measurements made by Diat *et al.*[33,61] and Safinya et al.[62] While the symmetry of this radial scattering bears a resemblance to the scattering expected from an a oriented lamellar phase (Figure 3b), the strong peak scattering expected from an aligned lamellar phase is absent. Of themselves, these observations do not provide clear evidence of the nature of the structural changes in the fluid.

Our SANS measurements in the tangential geometry provide a striking indication of the new ordering of the system under shear in region II. At low shear, the rather smaller effective sample volume gives a weaker but still clearly isotropic signal corresponding to that in the radial geometry. As the shear rate increases, the scattering becomes increasingly anisotropic. For an a oriented lamellar phase, we would expect to observe similar scattering patterns in both geometries. However, in the tangential geometry, the scattering, while again weakening in the vorticity direction, actually increases in the velocity gradient direction. For $\dot{\gamma} \sim 850$ s^{-1}, a distinct Bragg peak is seen along $Q_{\nabla V}$, clearly indicating the formation of a shear-induced lamellar phase in the c orientation (Figures 11 and 3b). This Bragg peak signal is clear evidence of a shear-induced sponge to lamellar transformation. It continues to increase in region II and eventually saturates at $\dot{\gamma} \sim$2000 s^{-1}, corresponding to the disappearance of scattering in the Q range of the sponge pore correlation peak in the radial scattering configuration measurements—indicating that the sample has been totally transformed. Scattering data for this Bragg saturation region are shown for $\dot{\gamma} \sim 2700$ s^{-1}. In this region we also note the emergence of scattering at lower Q values visible as a ring around the beam stop. In the radial geometry measurements, we also see an increase in scattering at low Q at this shear rate, but only in the vorticity (Z) direction.

After a gradual increase and the stability of the saturation region, the transition to the quasi-Newtonian region III is marked by a falloff of the shear-induced lamellar Bragg scattered intensity. In the tangential configuration scattering pattern for $\dot{\gamma} \sim 3700$ s^{-1}, the Bragg signal has fallen to about one-half from its strength at $\dot{\gamma} \sim 2700$ s^{-1}, and it entirely disappears by $\dot{\gamma} \sim 5000$ s^{-1}. The final scattering patterns, represented here by the data for $\dot{\gamma} \sim 9600$ s^{-1}, are dominated by the increase of the low Q scattering first visible in the $\dot{\gamma} \sim 2700$ s^{-1} data: a ring near the beam stop in the tangential data and similar strong scattering in the vorticity (Z) direction in the radial data.

To quantify the structural response of this system to shear, we define I_Z, I_V, and $I_{\nabla V}$, the corrected SANS intensities averaged over sectors within ±10° of respectively the Z, V, and ∇V directions. The results of this analysis are presented in Figure 11. Scattering intensities along the flow direction, I_V, and the velocity gradient direction, $I_{\nabla V}$, are obtained from radial and tangential measurements, respectively. Scattering along the vorticity direction, I_Z, is obtained from both radial and tangential geometries. Note that, as should be the case, the I_Z scattering values (open symbols) obtained from both geometries are the same at all shear rates. This demonstrates the consistency of the method used to absolutely normalize the data outlined in the Experimental Section.[43]

In the isotropic scattering from the sponge at rest, the sector intensities $I_Z(Q)$, $I_V(Q)$, and $I_{\nabla V}(Q)$ are of course identical and all show the characteristic broad correlation peak related to the sponge pore size. For this sample the correlation peak scattering occurs at $Q_3 \sim 0.008$ Å^{-1}, corresponding to a pore size of ~800 Å. As the shear increases, the correlation peak diminishes in intensity and eventually disappears in both Z and V directions, while becoming more pronounced and shifting toward higher wave vectors in the ∇V direction to finally form a (quasi-Bragg) peak in $I_{\nabla V}$ at $Q_L \sim 0.010$ Å^{-1}, corresponding to a smectic periodicity of 630 Å. This feature is clearly visible in these data for shear rates between 850 and 2700 s^{-1}. As might be expected, the ratio between the sponge phase correlation length and the induced lamellar periodicity is about 1.25, the same ratio as obtained in static SANS measurements at thermodynamic equilibrium between sponge and lamellar phases at the same membrane volume fraction.[26,63] The low Q scattering in region III is visible in strong and equal signals in I_Z and $I_{\nabla V}$ for the $\dot{\gamma} \sim 9600$ s^{-1} data. The intensity of these signals is still increasing rapidly with decreasing scattering vector at the low Q limit of these scattering measurements (~0.004 Å^{-1}**),** indicating the formation of structures rather larger than the sponge pore size or shear-induced lamellar periodicity.

Scaling Behavior of the Sweetened Sponge Response to Applied Shear. Since the dextrose in this system is taken up exclusively by the brine solvent, we can readily and independently vary the CPCl/hexanol membrane volume fraction and the dextrose/brine solvent viscosity to investigate not just individual sample responses as previously reported in the literature[32,34,38] but the full scaling behavior of the shear response in these systems with respect to these parameters. Figure 12a shows the viscosity versus shear behavior of the two dilute sponge in light brine sample series corresponding to the heavy brine samples for which equilibrium scattering data scaling was presented in Figure 6: (i) constant $\phi = 0.05$, with varying $\psi = 0$, 0.2, 0.3, and 0.4, for which the corresponding solvent viscosities η_s are 1.0, 2.8, 5.6, and 13.4 cP; and (ii) constant high dextrose volume fraction $\psi = 0.4$ ($\eta_s = 13.4$ cP) and varying $\phi = 0.03$, 0.05, 0.07, and 0.10. The low shear rate viscosity measured for these seven samples varies by an order of magnitude, while the onset of shear thinning varies by nearly 2 orders or magnitude. We can see that all the curves show the same general response but at different shear rate values. The two series clearly and immediately demonstrate the

(61) Diat, O. Thesis no. 833, University Bordeaux I, France, 1992.
(62) Plano, R. J.; Safinya, C. R.; Sirota, E. B.; Wenzel, L. J. *Rev. Sci. Instrum.* **1993**, *64*, 1309.
(63) Porte, G.; Marignan, J.; Bassereau, P.; May, R. *J. Phys. (Paris)* **1988**, *49*, 511.

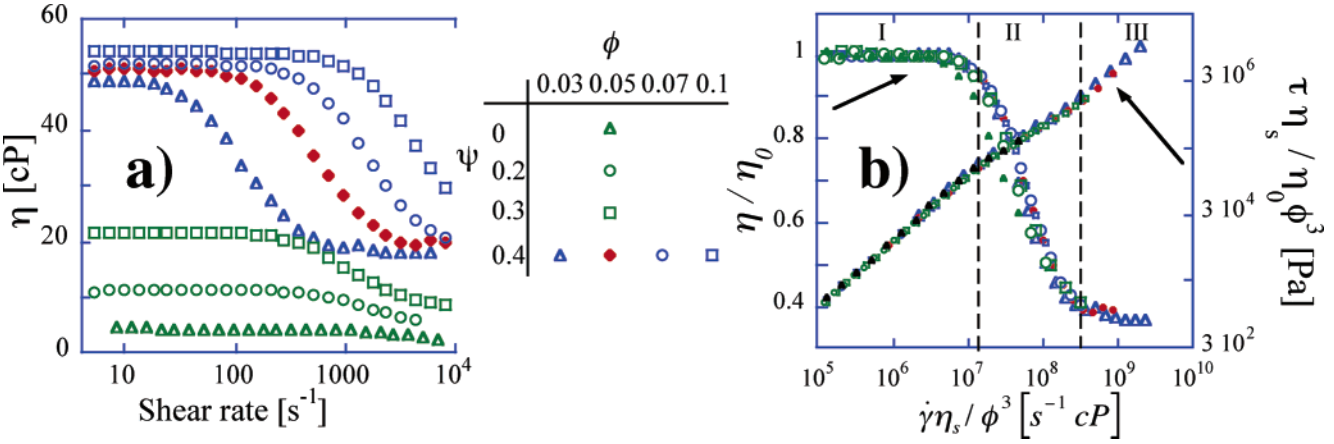

Figure 12. (a) Variation of the viscosity η versus shear $\dot{\gamma}$ for the light brine sponge sample series: at constant membrane volume fraction $\phi = 0.05$ and varying dextrose concentration (and solvent viscosity η_s) $\psi = 0$, 0.2, 0.3, and 0.4; and at constant high dextrose concentration $\psi = 0.4$ and varying membrane volume fraction $\phi = 0.03$, 0.05, 0.07, and 0.10. (b) The same data presented as the viscosity ratio η/η_0 (left-hand scale), where η_0 is the extrapolated zero shear viscosity, versus the rescaled shear rate $\dot{\gamma}\eta_s/\phi^3$, showing master curve behavior. The right-hand scale shows the corresponding master curve behavior of the shear stress rescaled as $\tau(\eta_s/\eta_0)/\phi^3$. Dotted vertical lines show the nominal boundaries of the three shear response regions discussed in the text.

Table 2. Sample Parameters and Corresponding Shear Response Scaling Factors for Rheological Series in Light Brine and Corresponding Scattering Series in Heavy Brine

ϕ	ψ	$\eta_s(H_2O)$ (cP)	$\eta_s(H_2O)/\phi^3$ (cP)	$\eta_s(D_2O)$ (cP)	$\eta_s(D_2O)/\phi^3$ (cP)
0.03	0.4	13.4	5.0×10^5	16.2	6.0×10^5
0.05	0.4	13.4	1.1×10^5	16.2	1.3×10^5
0.05	0.3	5.5	4.4×10^4	6.7	5.4×10^4
0.07	0.4	13.4	3.9×10^4	16.2	4.7×10^4
0.05	0.2	2.7	2.2×10^4	3.3	2.2×10^4
0.10	0.4	13.4	1.3×10^4	16.2	1.6×10^4
0.05	0	1.0	8.0×10^3	1.2	9.6×10^3

expected trends: that required shear rates for the shear-thinning behavior are lowered as membrane volume fractions decrease or sample viscosities increase.

We now compare the rheological behavior in this system with the expected scaling behavior. The left-hand scale in Figure 12b corresponds to the normalized sample viscosity η/η_0, where η_0 is the zero shear viscosity (obtained by extrapolation) versus a rescaled shear rate $\dot{\gamma}\eta_s/\phi^3$—essentially a scaled Deborah number. (The values of the scaling factor η_s/ϕ^3 for these series, which vary by nearly 2 orders of magnitude, are listed in Table 2.) As we can see, all the curves are now closely superimposed on a rheological "master" curve with, overall, the same three well-defined regions of the shear response described above. All three regimes are only clearly observed for the most dilute samples with high solvent viscosity because of the mechanical limitations of the rheometer. Vertical dotted lines indicate nominal boundaries of the shear regions, the region I/II boundary at $\dot{\gamma}\eta_s/\phi^3 = 1.4 \times 10^7$ s^{-1} cP, and that for II/III at $\dot{\gamma}\eta_s/\phi^3 = 3.5 \times 10^8$ s^{-1} cP. Also plotted on this graph (right-hand scale) are correspondingly rescaled shear stress curves $\tau(\eta_s/\eta_0)/\phi^3$. These too show clear master curve behavior. From these master curves we see that viscosity and stresses again vary smoothly over the shear-thinning region II, indicating that the samples are not biphasic in this region and that the transition is not first-order.[58,59]

To quantify the scaling dependence of the "critical shear rate" on these parameters in Figure 13, we plot the crossover shear rate ($\dot{\gamma}_{I/II}$) between regime I and regime II, quantified as the point at which shear thinning has reduced the sample viscosity to 95% of its zero shear limit in a log−log representation against ϕ/η_s. For a series of

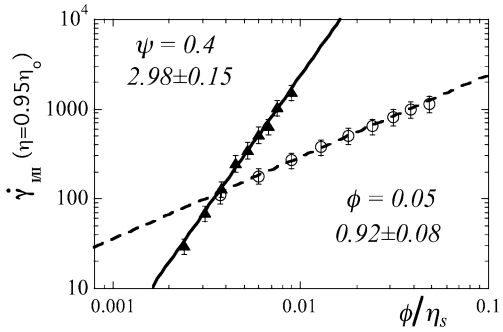

Figure 13. Scaling exponents of the shear response in the sweetened sponge systems determined from variation of the position of the region I/II boundary (defined as the point where the viscosity has fallen to 95% of its zero shear viscosity η_0) versus ϕ/η_s for two sponge phase sample series: (▲) constant dextrose volume fraction and solvent viscosity $\psi = 0.4/\eta_s = 13.4$ cP for varying membrane volume fractions ϕ; and (○) constant membrane volume fraction $\phi = 0.05$ for varying dextrose concentrations and viscosities $\eta_s = 1.0-13.4$ cP.

membrane volume fractions at $\psi = 0.4$ ($\eta_s = 13.4$ cP), we find excellent agreement with the predicted ϕ^3 behavior, obtaining an exponent of 2.98 ± 0.15. The result for the constant membrane volume fraction $\phi = 0.05$ series with varying solvent viscosity is nearly as good, with the expected $1/\eta_s$ dependence being unity to within the error limits of the experimentally determined exponent of 0.92 ± 0.08.

The structural response of all seven samples in the heavy brine sample series [(i) constant $\phi = 0.05$, with varying $\psi = 0$, 0.2, 0.3, and 0.4, for which the corresponding solvent viscosities η_s are 1.2, 3.3, 6.7, and 16.2 cP; and (ii) constant high dextrose volume fraction $\psi = 0.4$ ($\eta_s = 16.2$ cP) and varying $\phi = 0.03$, 0.05, 0.07, and 0.10] may be quantified in terms of the variation of the anisotropy parameters in the scattering patterns. For the (Z, V) and (Z, ∇V) plane scattering data collected in the radial and tangential configurations, respectively (Figure 3a), the corresponding anisotropy parameters are conventionally defined[33] as the intensity contrast between the perpendicular directions for the two geometries as

$$A_{RAD} = \left|\frac{I_V - I_Z}{I_V + I_Z}\right| \quad \text{and} \quad A_{TAN} = \left|\frac{I_{\nabla V} - I_Z}{I_{\nabla V} + I_Z}\right| \qquad (4)$$

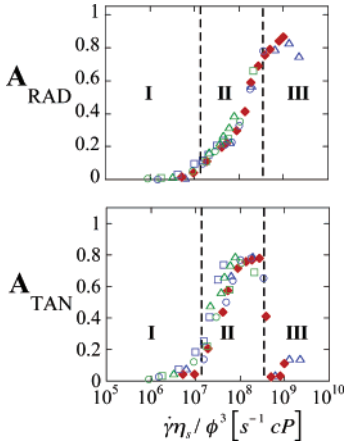

Figure 14. Master curve variation with the rescaled shear rate $\dot{\gamma}\eta_s/\phi^3$ of the SANS anisotropy parameters defined in the text from radial, (a) A_{RAD}, and tangential, (b) A_{TAN}, configuration scattering data. The two heavy brine sample series shown are the same as those for which the scaling of static SANS data was shown in Figure 6—constant $\phi = 0.05$ and $\psi = 0$, 0.2, 0.3, and 0.4; and constant high dextrose concentration $\psi = 0.4$, and $\phi = 0.03$, 0.05, 0.07, and 0.10—and correspond to the light brine sample series for which rheological master curves are shown in Figure 12. As described in the text, the behavior of the anisotropy parameters closely corresponds to the rheological response. The vertical dotted lines show the nominal shear response region boundaries discussed in the text at the same values of $\dot{\gamma}\eta_s/\phi^3$ at which they were shown in the rheological measurements shown in Figure 12.

To track the sample anisotropy at length scales characteristic of the sponge and lamellar phases, these parameters are evaluated in the region of the sponge correlation peak $Q_3 \sim 2\pi/\xi$. Figure 14 shows the variation of these parameters for a range of membrane volume fractions at different dextrose content ψ against the same rescaling of the shear rate $\dot{\gamma}\eta_s/\phi^3$ used for the light water rheological series measurements. Again, for the full sample series we see that the shear response follows a master curve dependence on $\dot{\gamma}\eta_s/\phi^3$, as was observed for the rheological measurements. (The values of the scaling factor η_s/ϕ^3 for these series are listed in Table 2.) The dotted line boundaries between the regions are drawn at the same values of $\dot{\gamma}\eta_s/\phi^3$ as they were for the rheological measurements shown in Figure 12 and indicate that the variation of these microscopic anisotropies closely corresponds to the macroscopic rheological observations. In the zero and low shear region I, both A_{RAD} and A_{TAN} are zero, indicating an isotropic structure. In region II, both anisotropy parameters begin to increase. For A_{TAN} this is due to the shear-induced formation of lamellar phases with membrane normals oriented parallel to the velocity gradient (c orientation), giving rise to strong Bragg scattering in the ∇V direction. In this region A_{RAD} also increases, but more slowly—despite an overall loss of scattering intensity in the radial scattering geometry scattering patterns. This is due to scattering in the vorticity (Z) direction decreasing more slowly than the scattering along the flow (V) direction (see Figure 11).

To further follow the details of the development and eventual collapse of the shear-induced lamellar phase in Figure 15, we plot correlation peak position and intensity variation with $\dot{\gamma}\eta_s/\phi^3$ for two of the three high dextrose heavy brine samples for which region III is experimentally accessible. These are the $\phi = 0.05/\psi = 0.4$ and $\phi = 0.07/\psi = 0.4$ samples. (The sponge correlation peak for the other sample spanning regions II and III, the $\phi = 0.03/\psi = 0.4$ sample, is too close to the beam stop in our data for its position to be accurately determined.) As in Figure 6, we

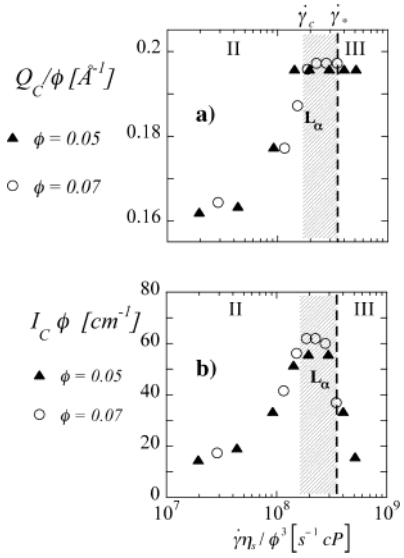

Figure 15. Correspondence of correlation peak position and scattering intensity variation versus rescaled shear rate $\dot{\gamma}\eta_s/\phi^3$ for the $\phi = 0.05/\psi = 0.4$ and $\phi = 0.07/\psi = 0.4$ sponge samples in regions II and III. The peak position is shown in part a as Q_C/ϕ, and the intensity in part b, as $I_C\phi$ to remove the membrane phase scaling (see also Figure 6). The shading in part b indicates the saturation plateau in $I_Q\phi$ of the shear-induced lamellar phase signal, and the vertical dotted line shows the region II/III boundary at the $\dot{\gamma}\eta_s/\phi^3$ value for its collapse.

can, as a direct consequence of the scale invariance of membrane phase structures, conveniently compare the responses of these two samples by plotting in Figure 15a the rescaled wave vector of the correlation peak position as Q_C/ϕ and in Figure 15b the rescaled correlation peak intensity along the shear gradient direction direction (∇V) as $I_C\phi$ with respect to $\dot{\gamma}\eta_s/\phi^3$. From Figure 15 it is evident that, like the anisotropy parameters for the complete series, both Q_C/ϕ and $I_C\phi$ for these samples increase gradually over region II, indicating a continuous process as the membrane-forming surfactants are excluded from forming channels and confined to oriented lamellar sheets. This is consistent with the absence of a rheological stress plateau in the rheological measurements and demonstrates from a microstructural perspective that the transformation cannot be first-order. All three direct indicators of the lamellar phase reach plateau values within region II. Q_C/ϕ and $I_C\phi$ for $\dot{\gamma}\eta_s/\phi^3 \approx 2 \times 10^8$ s^{-1} cP, while A_{TAN} reaches its saturation value of ~0.8 somewhat earlier for $\dot{\gamma}\eta_s/\phi^3 \approx 7 \times 10^7$ s^{-1} cP, as strong scattering from even a partially aligned state dominates the anisotropy of the scattering patterns. The saturation of $I_C\phi$ due to strong scattering indicates a complete alignment of the shear-induced lamellar phase. Comparing the two sample responses in Figure 15, we see that the total increase in Q_C/ϕ is about 25%, from the initial value at $Q_3/\phi \sim 0.16$ Å^{-1} for the sponge correlation ring to $Q_L/\phi \sim 0.20$ Å^{-1} for the smectic Bragg peak from the saturated shear-induced lamellar phase. As was noted for the full presentation of the $\phi = 0.05/\psi = 0.4$ scattering data in Figure 11, this is the same wave vector ratio as is observed between static SANS measurements of sponge and lamellar samples in this system.[26,48,49]

Just below the nominal region II/III boundary at $\dot{\gamma}\eta_s/\phi^3 = 3.5 \times 10^8$ s^{-1} cP, for A_{TAN}, Q_C/ϕ and $I_C\phi$ are at their saturation values, as finally is A_{RAD}, also at a value of ~0.8. The latter is driven not by lamellar phase scattering but by an increase in low Q vorticity (Z) direction scattering from larger scale structures overwhelming an almost total loss of scattering signal along the flow (V) direction. As

the region III boundary is passed, two of the lamellar phase ordering indicators, $I_C\phi$ and A_{TAN}, fall dramatically. Their rapid decline signals a transformation of the shear-induced lamellar phase. A_{TAN} falls to a value of ~0.1 as strong isotropic scattering emerges for the radial configuration data at low Q, while, despite the noticeable increase in the vorticity (Z) direction at low Q, A_{RAD} cannot increase significantly above the saturation value of about ~0.8 it has already attained. Note, however, in contrast to the case for the initial shear-induced alignment, the peak position does not change immediately as the intensity falls, as the rescaled peak position Q_C/ϕ stays near the smectic Bragg value ~0.2 Å^{-1}, somewhat beyond the region II/III boundary for the $\phi = 0.05/\psi = 0.4$ and $\phi = 0.07/\psi = 0.4$ samples, indicating that some fraction of the lamellar phase persists through this process. This is most clearly seen in the tangential configuration scattering pattern in Figure 11 for the $\phi = 0.05/\psi = 0.4$ sample data shear rate just beyond collapse, $\dot\gamma = 3700$ s^{-1} ($\dot\gamma\eta_s/\phi^3 = 4.03 \times 10^8$ s^{-1} cP)—as collapse proceeds (the Bragg intensity has fallen by 50% from the saturation value), the lamellar peak scattering coexists with the strong scattering at small Q from whatever structure is now being formed. It seems that, unlike the shear-induced lamellar transformation itself, the shear-induced collapse is a quasi-first-order process.

Discussion

Scaling of the Shear Response of the Sweetened Sponge Phases. Altogether these results present clear evidence that a sponge to lamellar transformation can be induced by shear flow in these sponge systems. For both rheological and SANS data, the master curves presented above against the rescaled shear rate $\dot\gamma\eta_s/\phi^3$ indicate good agreement with the expected scaling behavior of the sponge phase response to shear. As well as can be determined from the limited number of samples for which our region III is experimentally accessible, this scaling continues to the final collapse of the shear-induced lamellar phase.

One question which is occasionally raised with respect to membrane phase fluid dynamics is whether the solvent viscosity η_s or the sample viscosity, that is, η_0, is the relevant scale viscosity to employ in treatments of shear flow responses in membrane systems. It has been usual to employ the solvent viscosity to estimate viscous dissipation,[64−66] the assumption being the motion of the more fluid solvent as modified by geometric constraints presented by the membrane structure may be treated in a manner analogous to flow in porous media. However, Bruinsma and Rabin[67] used the sample viscosity in their theory of the dynamics of lamellar phase shear response, as did Zilman and Granek[68] to explain lamellar to spherulite transitions in surfactant systems. More recently, Al kahwaji and Kellay[69] found that the onset of turbidity and increased small angle light scattering in freely suspended thin films under shear that they interpreted as a signature of lamellar collapse scaled inversely with the lamellar phase viscosity rather than the solvent viscosities in their AOT and $C_{12}E_5$ membrane lamellar phases.

In the treatment of the low shear rheology of these dilute systems above, we found that the simple constraint to solvent flow presented by the membrane geometry of the sponge labyrinth dominates the sample viscosity at low shear rates, that is, $\eta_0 \approx A\eta_s$, with a relatively small membrane volume fraction dependent contribution. While this essentially embodies the assumption which has motivated the choice of the solvent viscosity scaling, it also limits the usefulness of these systems in addressing this question. Thus, we found that nearly equivalent master curve rescaling to those shown for the rheology in Figure 12b and the scattering data in Figures 14 and 15 with respect to the solvent viscosity η_s can in fact be produced with respect to the zero shear rate viscosity η_0, that is, versus a rescaled shear rate parameter $\dot\gamma\eta_0/\phi^3$. The normalization of the shear stress corresponding to the viscosity normalization of η/η_0 in the equivalent of Figure 12b is then τ/ϕ^3, rather than $\tau(\eta_s/\eta_0)/\phi^3$. Using the same data for the $\dot\gamma_{I/II}$ as those of Figure 13 plotted against ϕ/η_0, we obtained a similar value for the expected coefficient of viscosity of 0.95 ± 0.08, although the coefficient for ϕ was 3.29 ± 0.15, nearly two standard deviations beyond the expected value. Examination of Figure 7 will show that this scaling equivalence is simply due to the fact that although the values of η_0 and η_s vary by more than an order of magnitude for the two series presented in Figure 13, $\phi = 0.05/\psi = 0-0.04$ and $\phi = 0.03-0.10/\psi = 0.4$, which cover the full range of samples with critical shear rates $\dot\gamma_{I/II}$ accessible with our rheometer, their ratio η_0/η_s varies by less than 20%. The variation is even less between those samples with comparable scaling factors and thus significant data overlap.

Nature of the Shear-Induced Lamellar Phase Transformation. Despite the good agreement with the scaling predictions, two important aspects of our experimental observations depart both from the theoretical picture presented by Cates and Milner and from results reported for isotropic diblock systems to which their theory has also been applied.[60] First, they predicted an a orientation of the shear-induced lamellar phase, with membrane normals in the vorticity direction, rather than the c orientation, with membrane normals along the flow gradient direction, we observed in our system. Yamamota and Tanaka[32] also observed c orientations for their $C_{12}E_5$ sponges under oscillatory Poiseuille shear. In the case of this aspect of the sponge response, we note that a sponge membrane does not establish a connection between regions of solvent that it separates, which are able to flow freely on either side. In the isotropic diblock phase investigated by Koppi et al.,[29] which did show the a orientation, the interfacial region represents a physical connection between regions rich in the two polymer species. This might tend to favor the a orientation lamellar structure, since adjacent layers are moving together in the flow field.

Second, Cates and Milner suggested that under shear the isotropic phase should separate into coexisting isotropic and lamellar phases over some intermediate flow regime before a uniform lamellar phase is formed at high shear. We saw no evidence of phase coexistence, a signature of a first-order transition, in these measurements. The absence of a stress plateau in the corresponding shear-thinning rheological regime together with the absence of hysteresis and the gradual increase of the aligned correlation peak intensity (Figures 11 and 15a) and its continuously shifting position indicate a progressive transformation from sponge to lamellar order as membrane-forming material is excluded from channels and confined to more oriented membranes—finally forming stacked sheets. Since a c oriented shear-induced lamellar phase does not contribute to the scattering in the radial geometry, coexistence of sponge and shear-induced lamel-

(64) Martin, P. C.; Parodi, O.; Pershan, P. S. *Phys. Rev. A* **1972**, *6*, 2401.
(65) Brochard, F.; de Gennes, P. G. *Pramana, Suppl.* **1975**, *1*, 1.
(66) Nallet, F.; Roux, D.; Prost, J. *J. Phys. (Paris)* **1989**, *50*, 3147.
(67) Bruinsma, R.; Rabin, Y. *Phys. Rev. A* **1992**, *45*, 994.
(68) Zilman, A. G.; Granek, R. *Eur. Phys. J. B* **1999**, *11*, 593.
(69) Al kahwaji, A.; Kellay, H. *Phys. Rev. Lett.* **2000**, *84*, 3073.

lar phases in our Couette cell would simply present an isotropic sponge scattering pattern in the radial geometry, simultaneously with lamellar Bragg scattering against a weaker isotropic background in the tangential geometry. Further, the completely reversible transformations we observed showed no appreciable hysteresis. The time resolution limit of the SANS data collection scheme employed in these measurements was about 1 min. Within this time after the cessation of shear, Bragg scattering from shear-induced lamellar phases gave way completely to the isotropic scattering characteristic of the sponge structure. On similar time scales, we observed no history effects upon repeating rheological measurements of samples previously sheared to the shear-thinning regime II.

In the initial Newtonian region (I), there is no discernible change in the isotropic scattering ring from the sponge phase (hence, no structural changes), as the shear rate is well below the membrane response frequency, τ_3^{-1} ($De \ll 1$), allowing ample time for stress relaxation in the system by simple diffusion. In the shear-thinning region (II), as the shear rate approaches this frequency ($\dot{\gamma} \rightarrow \sim\tau_3^{-1}$, $De \rightarrow 1$), the isotropic structure is then progressively stretched in the flow direction, as total dissipation of the shear-induced stresses can no longer be achieved. The continuous nature of the transformation may to some extent be reconciled with a quasi-thermodynamic picture by considering that in the continuously fluctuating sponge system the opportunity for sponge handle creation (or destruction) between membranes will be offered on something like the frequency. The density of connections or handles in the gradient direction (∇V) will decrease if the energy cost of the stretched membrane passages in this direction increases. As this cost approaches and exceeds that of the lamellar state configuration for adjacent membranes, this would lead to the progressive development of a smectic order in the observed c orientation, as passages are less likely to be created (or recreated) in this direction with membranes moving past each other at ever increasing speeds, $\sim\dot{\gamma}\xi$. In the a orientation adjacent membranes are moving together in the flow field, so no such relative velocity effects will hamper the reformation of passages in the vorticity direction. The shear-thinning response we observe is consistent with the microscopic structural change to this increasingly anisotropic sheared sponge structure. Membranes aligned with their normals aligned along the flow gradient direction can slide past each other easily in the Couette flow field. At some point, the thermodynamic rate of disruption of passages connecting membrane sheets along the flow gradient direction will exceed the limit at which diffusive membrane motions allow them to be re-established, so the fully aligned shear-induced lamellar phase characterized by the saturation of the scattered intensity $I_{\nabla V}$ at the final peak position Q_L is formed.

Collapse of the Shear-Induced Lamellar Phase. The fully aligned shear-induced phase is maintained over only a narrow range of the higher shear rates in region II (shaded region in Figure 15b). At the highest shears in region III, the shear-induced lamellar phase becomes unstable. Although the position of the Bragg peak does not shift, a sharp drop in $I_{\nabla V}$ at the onset of region III signals the disappearance of this shear-induced lamellar phase. Rheologically the solution becomes "quasi"-Newtonian at a roughly constant viscosity, rather lower than that of the low shear region I. Structurally the shear-induced lamellar phase gives way to a structure with correlations on a much longer length scale with strong scattering at low Q (close to the beam stop in all our measurements). The coexistence of the shear-induced Bragg scattering signal with this low Q scattering suggests that the transition may be quasi-first-order. The isotropy of the tangential scattering and the strong anisotropy of the radial pattern (see Figure 11, $\dot{\gamma} = 9600\ s^{-1}$) clearly suggest that the large scale organization of material in region III has cylindrical symmetry about the flow axis, V. However, the continuing rise in intensity to the lowest Q values attained here does not reveal any length scales for the shear-induced structures involved. Unfortunately our current data on a limited number of samples do not cover this region in sufficient detail or over a wide enough range of length scales to allow us to fully determine the nature of the transition and of the final structures being formed.

However, the data presented here do allow us to rule out two suggested explanations of these high shear rate observations fairly easily. The first is hydrodynamic—that we are simply observing turbulent breakup of the lamellar phase. For the outer cylinder rotation used for our Couette shear cell, the turbulence regime is reached at a critical Reynolds number above about 1500. In the present case, due to their high viscosities, this would not be expected for any of our $\psi = 0.4$ samples at shear rates below $\sim$50 000 s^{-1} (well beyond the range presented here and the operational limits of our shear cell[43]). Also, turbulent flow would result in an increase in the apparent viscosity, which we do not observe, and would be expected to lead to fully isotropic scattering, whereas at the highest shear rates our radial scattering patterns remain strongly anisotropic (see Figure 11, $\dot{\gamma} = 9600\ s^{-1}$). A second possibility that the final large scale structures are the spherulites or multilamellar vesicles[11−14,18] often encountered when lamellar phases are subjected to high shear rates is ruled out by the absence of their characteristic Bragg peaks in either radial or tangential configurations.

While the word "collapse" is apposite to describe the rapid disappearance of the shear-induced lamellar phase at the onset of region III, it is also suggested by the following interpretation of that behavior. When undulation forces stabilize a lamellar structure, it has been theoretically predicted that the phase should collapse when the intermembrane resistance to compression vanishes, as shearing flow suppresses fluctuations. This mechanism is a logical extension of the sponge-to-lamellar transition itself, which occurs by suppression of membrane fluctuations in the ∇V direction in the isotropic phase. Lamellar collapse was predicted by Ramaswamy[70] for shear rates larger than a critical value $\dot{\gamma}^* \sim (k_B T)^3/\kappa^2\eta_s d^3$, where κ is the membrane bending modulus and d is the separation of adjacent bilayers. For CPCl/hexanol membranes, κ has been experimentally determined[26,49,71] to be $\approx 1 k_B T$ at room temperature, so we have $\dot{\gamma}^* \sim k_B T/\eta_s d^3$. This critical shear rate follows the same scaling dependence as $\dot{\gamma}_c$, but with a different characteristic distance. Since $d = 2\pi/Q_L$ and assuming a rough equality of the respective prefactors, we might expect $\dot{\gamma}^*/\dot{\gamma}_c \sim (\xi/d)^3 = (Q_L/Q_3)^3$. For our observed scattering peaks, $(Q_L/Q_3) \approx 1.25$, so $\dot{\gamma}^*/\dot{\gamma}_c \sim 2$. This is close to the observed width of the stable region of the saturated shear-induced lamellar phase (the shaded $I_C\phi$ plateau region in Figure 15b) before it collapses at higher shear.[72] With respect to the narrowness of this window of stability, we note that Bruinsma and Rabin[67] speculated that

(70) Ramaswamy, S. *Phys. Rev. Lett.* **1992**, *69*, 112. Note that the actual expression given in this reference is typographically incorrect. Ramaswamy, S. (private communication).

(71) Bouglet, G.; Ligoure, C.; Bellocq, A. M.; Dufourc, E.; Mosser, G. *Phys. Rev. E* **1998**, *57*, 834.

lamellar collapse might preclude the shear-induced sponge to lamellar transformation altogether.

Conclusion

In this work we have shown that dextrose dissolved in the brine solvent of a CPCl/hexanol/brine system has little effect on the equilibrium phase behavior of this system. More particularly, the dextrose is excluded from the structures formed by CPCl/hexanol, and our SANS measurements indicate that there is no significant effect on the membrane or equilibrium sponge phase morphology in this system due to this addition. However, while structural effects are minimal, order of magnitude changes may readily be made to the solvent viscosity and consequently the membrane dynamics. This strategy of adding an inert thickener to the solvent, which is simply excluded from the self-assembled structural components, may be of general utility in studies of the dynamics in this class of complex fluids. In the present case, it has allowed us to perform parallel SANS and rheological measurements of the shear response of the "sweetened" (CPCl)/hexanol/brine/dextrose sponges to unambiguously demonstrate that shearing these dilute sponge phases in a Couette cell induces a lamellar phase transformation in this system, as they shear thin. Further, the magnitude of the critical shear rates we observe for this transformation and more particularly their scaling with respect to membrane volume fraction and solvent viscosity are as expected from simple dimensional and fluid scaling arguments. Since the sponge systems studied are extremely sensitive to evaporation of the hexanol cosurfactant, our scattering experiments relied on the use of a newly designed Couette cell vapor barrier to maintain the sample within a small sealed volume. The overall consistency of the SANS measurements using this cell clearly suggests that earlier X-ray scattering effects interpreted as being due to a shear-induced first-order sponge to lamellar phase transition in this system at rather low shear for CPCl/hexanol/brine sponge samples without dextrose are simply composition driven, first-order transitions due to evaporation rather than the applied shear rate.

However, important details of the response we observe—clear c rather than a orientation of the shear-induced lamellar phase and complete suppression of the first-order nature of the equilibrium phase transition in this system (with no indication of first-order character observable in either rheological or microstructural measurements)—are not as predicted by Cates and Milner.[28] So, while their theory has been confirmed for some isotropic copolymer phases,[29] these observations and the varying details of shear responses from other topologically similar systems with differing relaxation paths[60] suggest that in its present form it cannot be applied straightforwardly to the class as a whole.

The significant slowing of the membrane dynamics achievable by the introduction of dextrose in the system allowed us to observe what is apparently the collapse of the shear-induced lamellar phase. To our knowledge, this is the first observation of collapse of a bulk lamellar phase.[73] The window of stability for the shear-induced phase before collapse occurs is in reasonable agreement with theoretical predictions of the relative scaling of these two processes for this system. That this window is open even so narrowly may be fortuitous; collapse would preclude lamellar saturation altogether for only relatively small changes in the bending modulus of the membranes. In other systems it is possible that the clear separation of the regimes we observe here may not be achieved. While scattering measurements from the three samples for which the collapse range of the rescaled shear parameter $\dot{\gamma}\eta_s/\phi^3 \sim 3.5 \times 10^8\ s^{-1}$ cP is accessible certainly suggest that this transition may be first-order, further detailed SANS and rheological measurements in this range will be necessary to confirm this and the exact nature of the large scale structures formed in this system at these shear rates.

Acknowledgment. Our thanks to J.B. Hayter, who initiated our work on the ORNL neutron scattering Couette shear cell; D. Glandon, B. Taylor, and R. Maples for their work on its various incarnations; C. Tsouris of ORNL for the use of his rheometer; B. Gu of ORNL for the use of his DLS instrument; J. P. Fluxench for the artwork of Figure 1; and G. Porte of the University of Montpellier, France, for fruitful discussions and helpful suggestions. Oak Ridge National Laboratory is managed by UT-Batelle LLC under Contract DE-AC05-00OR22725 for the U.S. Department of Energy. The NG3 SANS instrument at the National Institute of Standards and Technology Center for Neutron Research is supported by the U.S. National Science Foundation under agreement DMR-9986442. Identification of equipment or materials does not imply recommendation by NIST. P.D.B. acknowledges support as a NIST employee from NSF Grant DMR-9423101 during the early part of this study, and G.G.W. acknowledges that of the Australian Nuclear Science and Technology Organization and the Australian Research Council.

LA034661W

(72) Note that this theory too assumes lamellar phases in "a" orientation contrary to the "c" orientation we observe for the shear-induced phase. Nevertheless, the scaling laws involved will tend to be valid, since they are derived from a limited number of phase characteristics and hydrodynamic motions.

(73) Note that ref 69 claims to observe a shear-induced lamellar collapse on thin lamellar film.